

CHIMIKA CHRONIKA

NEW SERIES

AN INTERNATIONAL EDITION
OF THE ASSOCIATION OF GREEK CHEMISTS



3/95

CMCZ 24(3), 173-252(1995)

ISSN 0366-693X

Volume 24, No 3 p.p. 173-252 July-September 1995

CHIMIKA CHRONIKA

NEW SERIES

AN INTERNATIONAL EDITION

Published by the Association of Greek Chemists (A.G.C.)
27 Kaningos str. Athens 106 82 Greece

Journal Managing Committee, A.G.C.:

P.N. Dimotakis, D. Gegiou-Hadjoudis, D. Hadjigeorgiou-Giannakaki,
P.A. Siskos

Editor-in-chief: P.N. Dimotakis

Associate Editor: P.A. Siskos

Advisory Board: A. Evangelopoulos (National Hellenic Research Foundation), M. Georgiadis (Agricultural University), N. Hadjichristidis (University of Athens), N. Katsaros (NCSR "DEMOKRITOS"), D. Kyriakidis (University of Thessaloniki), M. Orfanopoulos (University of Crete), P. Papadopoulos (National Agricultural Research Foundation), F. Pomonis (University of Ioannina), N. Spirellis (Technical University of Athens), K. Tsiganos (University of Patras).

Foreign Advisors: P. Bontchev (Sofia), H. Işçi (Ankara), G.M. Milanovic (Belgrade), K.C. Nikolaou (Cyprus), E. Plasari (Tirana).

Correspondence, submission of papers, subscriptions, renewals and changes of address should be sent to Chimika Chronika-New Series, 27 Kaningos street, Athens 106 82, Greece. The Guide to Authors is published in the first issue of each volume, or sent by request. Subscriptions: 25 USD per year.

Phototypesetted and Printed in Greece by EPTALOFOS S.A.

12, Ardittou Str. 116 36 ATHENS Tel. 9217.513

Υπεύθυνος σύμφωνα με το νόμο: Ν. Κατσαρός, Κάνιγγος 27, Αθήνα 106 82.

Responsible under law: N. Katsaros, 27 Kaningos St., Athens 106 82, Greece.

Climate Forcing by Tropospheric Sulfate Aerosols Derived From Natural and Anthropogenic Sources.

N. MIHALOPOULOS* and B.C. NGUYEN

*Centre des Faibles Radioactivités, Laboratoire Mixte CNRS-CEA, Avenue de la Terrasse,
91198 Gif-sur-Yvette Cédex, FRANCE*

** University of Crete, Department of Chemistry, P.O Box 1470, 71409 Heraklion,
GREECE*

Received: February 27, 1995

SUMMARY

Gaseous sulfur compounds are emitted in the atmosphere from various natural and anthropogenic sources with dimethyl sulfide (DMS) and sulfur dioxide (SO₂) being the main representative sulfur compounds of natural and anthropogenic origin respectively. In the troposphere the gaseous sulfur compounds are finally oxidised to sulfate (SO₄²⁻). Through SO₄²⁻, sulfur gases may influence the earth's climate in two ways: a) directly, through scattering of solar radiation back to space and b) indirectly, through changes in cloud reflectivity brought by changes in the concentration of cloud condensation nuclei (CCN). Both ways lead to an increase of planetary albedo and thus exert a cooling influence on the planet. Based on empirical relations current climate forcing due to sulfate is to be -1.5 to -2.0 Wm⁻² globally averaged. This perturbation is comparable to current anthropogenic greenhouse gas forcing (~2.5 Wm⁻²) but opposite in sign. Thus forcing by sulfate aerosols could likely offset global greenhouse warming to a substantial degree.

Key words: aerosols, sulfate, sulfur dioxide, SO₂, dimethyl sulfide, DMS, atmospheric chemistry, sulfur cycle, climate, radiative forcing, greenhouse gases.

1. INTRODUCTION

During the last years considerable attention has been given to studying the response of earth's climate to perturbations in radiative forcing due to increased concentrations of infrared active (greenhouse) gases. Based on model calculations it is estimated that the increasing concentrations of carbon dioxide (CO₂), methane (CH₄), chlorofluorocarbons (CFC's) and nitrous oxide (N₂O) may produce a climate forcing of the order of 2.5 Wm⁻² from which 1.5 Wm⁻² is due to CO₂ (1).

On the other hand the earth's radiative budget is also influenced by the received solar energy which depends on astronomical cycles and the opacity of the atmospheric layer in the incident solar radiation. For example, during volcanic explosions when huge quantities

of aerosols are introduced into the stratosphere, a diminish of the earth temperature by 0.5 to 1°C has been observed. In addition, it has long been recognised that tropospheric aerosol particles can influence the radiative balance of earth both directly and indirectly (figure 1).

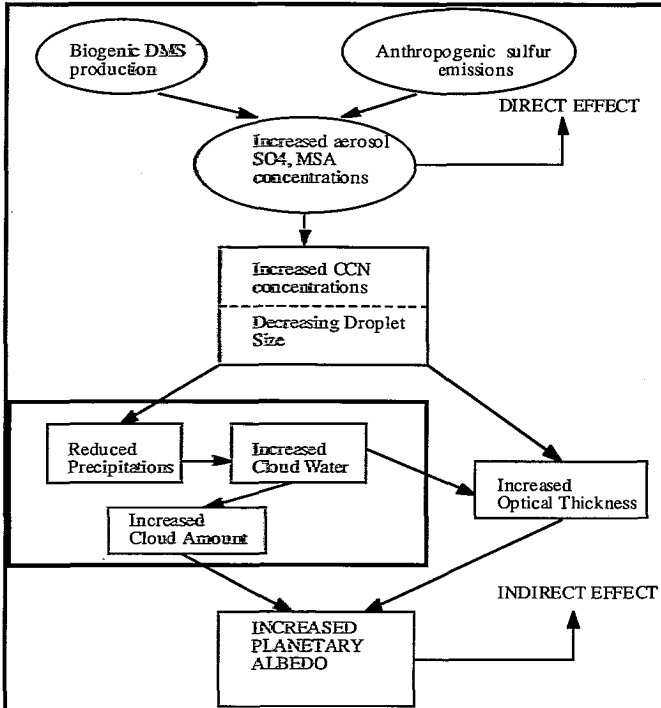


Figure 1: Pathways of direct and indirect influence of tropospheric sulfates on the earth's radiative budget. DMS= Dimethyl sulfide, MSA= Methanesulfonic acid, CCN= Cloud Condensation Nuclei.

Direct radiative influence: Aerosol particles influence the earth's radiative balance directly by back scattering and absorption of short-wave (solar) radiation. This role of aerosols is not new and was firstly pointed out in the early 1900's (2). Aerosol particles also absorb long-wave (infrared) radiation, but this effect is usually small (3).

In the unperturbed atmosphere, the principal aerosol constituents that contribute to light scattering are mainly sulfate aerosols produced from biogenic gaseous sulfur compounds especially over oceans although organic carbon from partial oxidation of gaseous biogenic organic compounds, such as terpenes (4) can also participate over continental areas covered by vegetation. In the polluted atmosphere the aerosols responsible for increased light scattering are produced by chemical reactions of sulfur-, nitrogen-, and carbon-, containing

gases, however, sulfur usually predominates. Other aerosol substances may also be locally important, especially sea-salt and those that are sporadic, such as from volcanoes, wildfires, as well as windblown dust from deserts, however their effects on the global climate are generally unimportant because the particles are large and usually short-lived and thus are transported only short distances.

Light absorption is dominated by particles containing elemental carbon, produced by incomplete combustion of carbonaceous fuel. The light-scattering effect is dominant at most latitudes, but absorption can dominate at high latitudes, especially over high reflective snow- or ice-covered surfaces and heavy industrialised regions (5).

Indirect radiative influence: Cloud droplets form in the lower atmosphere cloud condensation nuclei (CCN) by condensation of water on existing aerosol particles. Consequently, the concentration, size, and water solubility of the aerosol particles on which cloud droplets form CCN, have an immediate influence on the concentration and size of cloud droplets. Thus, increased concentrations of CCN result in increased concentrations of cloud droplets, enhancing short-wave albedo of clouds (figure 1) (6).

Sulfate aerosols appear to dominate anthropogenic influences on CCN, although particles of smoke from biomass combustion may be important in some circumstances. Thus sulfur containing tropospheric aerosol particles seem to be the most important among the tropospheric aerosols as radiative forcing agents.

In this article we present an overview on the current knowledge regarding the climatic effect of aerosol SO_4^{2-} . In order to better understand the distribution of aerosol SO_4^{2-} and how they can influence the earth's climate a short review on sulfur emissions and chemistry will be presented in the following paragraphs.

2. EMISSIONS AND ATMOSPHERIC CHEMISTRY OF SULFUR COMPOUNDS.

Emissions: Sulfur emissions from all sources are summarised in table 1. The distribution of sulfur sources among the two hemispheres is also presented.

TABLE 1. Global emissions of sulfur (TgS yr^{-1}) in the atmosphere in Northern Hemisphere (N.H) and Southern Hemisphere (S.H.)				
Source	Global	N.H	S.H.	Ref.
Anthropogenic (SO_2)	70	64	6	8, 9, 10
Biomass burning (SO_2)	2.5	1.1	1.4	11,12
Oceans (DMS)	16	6.9	9.1	13,14
Volcanoes (SO_2)	8.5	5.8	2.7	15
Soil and plants (reduced sulfur)	4	2.4	1.6	16, 17; 18

Sulfur DMS are the two most important sulfur compounds emitted from anthropogenic and natural sources respectively, with natural being the most important natural source. DMS is formed in surface seawater principally by the enzymatic cleavage of b-dimethylsulfonium-propionate (DMSP). Three biological processes are involved in the DMS production from phytoplanktonic DMSP: metabolic excretion, grazing and senescence, the two last processes being probably the major DMS sources (7). In the N.H. anthropogenic sulfur emissions exceed roughly by a factor of 10 natural sulfur emissions and account for about 94% of the global SO₂ emissions. In contrast, in the southern hemisphere (S.H.) the sulfur budget is dominated by natural sulfur emissions. Figure 2 presents the time history of the total anthropogenic SO₂ emissions. For comparison the estimates of global natural emissions of gaseous reduced sulfur compounds are also presented. Anthropogenic SO₂ emissions have roughly doubled over the last 30 years. It is worthwhile noting that although the estimates of the global anthropogenic sulfur emissions agree within ± 15%, the uncertainty in the estimate of the natural emission is of the order of a factor of two mainly due to the uncertainties in the emissions of DMS from the oceans.

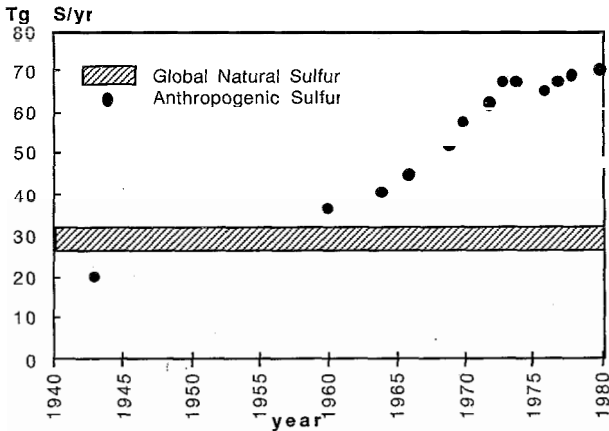


FIGURE 2: Time history of anthropogenic and natural gaseous sulfur emissions.

Dimethyl Sulfide: DMS is oxidised in the troposphere mainly through gas phase reactions with OH and NO₃ radicals. Reaction with OH radicals seems to be the most important oxidation pathway of DMS. Reaction with NO₃ radicals may be of importance during night time and when sufficiently high NO_x concentrations are present (> 10ppbv). Since the major emissions of DMS occur over the oceans, where NO_x concentrations are generally very low (< 0.1 ppbv), only over the oceans adjacent to the continents in the Northern

Hemisphere (NH) this reaction has an important role (19, 20).

The reaction of DMS with OH proceeds through two pathways: Abstraction of an H atom or addition of OH radical. The overall reaction rate decreases with increasing temperature and the branching ratio between the addition and the abstraction pathways is strongly temperature dependent: addition is favoured below 285 K and abstraction above this temperature. At present it is not clear whether each pathway leads to one major stable product or to a mixture of different products. Product studies indicate that SO₂, methanesulfonic acid (MSA), dimethylsulfone (DMSO) and dimethylsulfoxide (DMSO₂) are the major products (19). The possible pathways of the DMS + OH reaction are depicted in figure 3. Both laboratory and field studies have shown that SO₂ is the main product of the DMS/OH reaction with yield ranging up to 90% (21, 22, 23). For MSA, field studies show that it constitutes about 7% at low and mid latitudes and up to 50% at high latitudes (24, 25, 26). DMSO and DMSO₂ were observed both during laboratory and field studies, but their absolute yields are still very uncertain. Preliminary studies indicate that their combined yields account for about 15-20% (27).

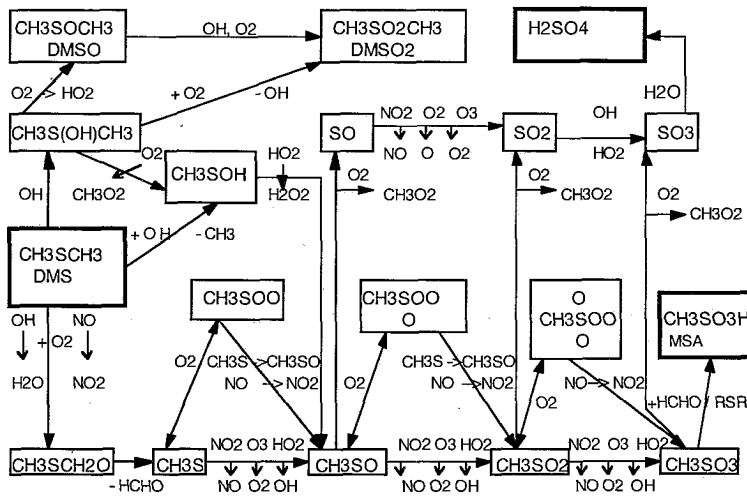
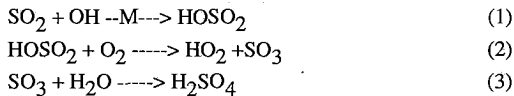


FIGURE 3: Possible pathways of DMS initiated oxidation by OH radicals.

Sulfur Dioxide: SO₂ is oxidised both in the gas- and liquid-phase to produce SO₄²⁻. In the gas phase SO₂ is assumed to react with OH radicals producing H₂SO₄ in a multi step reaction (28):



The first reaction is considered the rate determining. In the aqueous phase SO_2 is rapidly oxidised to SO_4^{2-} (at least 5-10 times faster than in gaseous phase) (29). The transformation of SO_2 to SO_4^{2-} is considered to proceed mainly through reactions with hydrogen peroxide (H_2O_2) and ozone but reactions with oxygen catalysed by metals such as manganese and iron may also be of importance in areas where the concentrations of those metals are high (29,30).

The major fate of sulfur compounds emitted to the atmosphere is oxidation to SO_4^{2-} . Based on model calculations (31), 55% of the SO_2 emitted or produced via oxidation of DMS and reduced sulfur species is oxidised to SO_4^{2-} , the remaining part being removed via dry (30%) or wet (15%) deposition.

3. ESTIMATES OF THE GLOBAL RADIATIVE FORCING PERTURBATION

Estimates of the global-average perturbation in radiative forcing induced by sulfate aerosols allow a comparison of the climatic influence of these aerosols with that due to increases in concentrations of CO_2 and other anthropogenic greenhouse gases. A doubling of global concentrations of CO_2 is thought (1) to contribute to an increase in long wave radiative forcing of the troposphere of $\sim 4.4 \text{ Wm}^{-2}$, and the increase from the preindustrial concentration of 280 ppmv to the 1990 value of 353 ppmv represents an increase of $\sim 1.5 \text{ Wm}^{-2}$. The total increase in forcing by all anthropogenic greenhouse gases over this period is estimated to have been 2.0 to 2.5 Wm^{-2} (1). We will use these numbers as a reference to assess the importance of the aerosol forcing. However, because of their different natures, the radiative forcing by sulfate aerosol should not be viewed as a simple compensation of greenhouse gas forcing (see paragraph dealing with future changes).

Contrary to the direct radiative influence which can be calculated using an empirical relationship of the optical effect with the aerosol burdens, it is not clear how to relate the mass concentration of SO_4^{2-} to CCN number concentration (indirect effect). Thus, the following calculations will include only the direct effect of aerosol back scatter of solar radiation.

3.1. Direct Forcing

The mean short wave forcing, ΔF_R , resulting from an increase in aerosol concentration can be expressed as:

$$\Delta F_R = -1/4 F_T (1-A_c) \Delta R_a \quad (4)$$

where, $1/4 F_T$ is the global mean top-of-the-atmosphere radiative flux, A_c is the fractional cloud cover, and ΔR_a is the perturbation in planetary mean albedo due to enhanced aerosol concentration (32). The factor $(1-A_c)$ is introduced because the albedo is enhanced mainly for non-cloud-covered portions of the planet. The negative sign denotes that the forcing

represents a cooling tendency. For an optically thin, light-scattering aerosol depth $da \ll 1$, ΔR_a is linear to the sulfate burden $B_{SO_4^{2-}}$ (gm^{-2}) and thus can be represented as:

$$\Delta R_a = K_1 B_{SO_4}$$

where K_1 can be assumed to be constant and equal to 2.04. For more details about K_1 and the empirical formula for direct radiative influence see (32,33).

However, since the SO_4^{2-} aerosol distribution is not homogeneous, e.g. anthropogenic SO_4^{2-} are largely confined to the N.H., a realistic estimation of the contribution of anthropogenic and natural sulfur sources to the global distribution of the reflected flux to space (ΔF_R) could be obtained only by the means of 3-dimensional models.

The global distribution of ΔF_R has been calculated by Charlson et al. (33), using a three-dimensional meteorological/chemical model (31). The model used in the simulations has a horizontal resolution of 10° longitude by 10° latitude and a vertical resolution of 10 layers between the surface and 100 hPa. Details regarding the transport and advection processes of the model are given in Zimmermann (34, 35) and Feichter and Crutzen (36). For the formulation of the sulfur scheme see Lagner and Rodhe (31). Emissions of sulfur species used are similar those listed in table 1.

The annual mean column burden SO_4^{2-} ($B_{SO_4^{2-}}$) in the troposphere is calculated for two different runs: including and neglecting natural emissions of sulfur. Figures 4a and 4b show the increase in reflected irradiance at the top of the atmosphere with actual cloud fraction being taken into account. Figure 4a shows ΔF_R including all emissions and figure 4b including only anthropogenic emissions. The maxima of loss of solar radiation in figure 4a indicate anthropogenic influence ranging from close to zero to over $4 Wm^{-2}$. We observe also that anthropogenic influence is limited only to the N.H.

Table 2 summarises the averaged reflected solar radiation due to tropospheric SO_4^{2-} (ΔF_R) for both hemispheres and both cases (with and without anthropogenic emissions). For comparison the radiative forcing perturbation due to increases in concentrations of CO_2 and other anthropogenic greenhouse gases is depicted. Changes in radiative forcing are of the same order of magnitude but of opposite sign to the changes due to the increase in CO_2 since pre-industrial times, which is estimated to cause a change in radiative forcing of $-1.5 Wm^{-2}$ (8). The change including all greenhouse gases is $-2.5 Wm^{-2}$ (8). The increase in

Table 2. Area averaged reflected solar radiation, ΔF_R (Wm^{-2}) due to tropospheric SO_4^{2-} .				
Area	ΔF_R anthropogenic + natural emissions	ΔF_R natural emissions	ΔF_R anthropogenic emissions	Forcing due to CO_2 (1.5) and all greenhouse gases (2.5)
N.H.	-1.57	-0.50	-1.07	1.5 (2.5)
S.H.	-0.46	-0.35	-0.11	1.5 (2.5)
Globe	-1.02	-0.42	-0.60	1.5 (2.5)

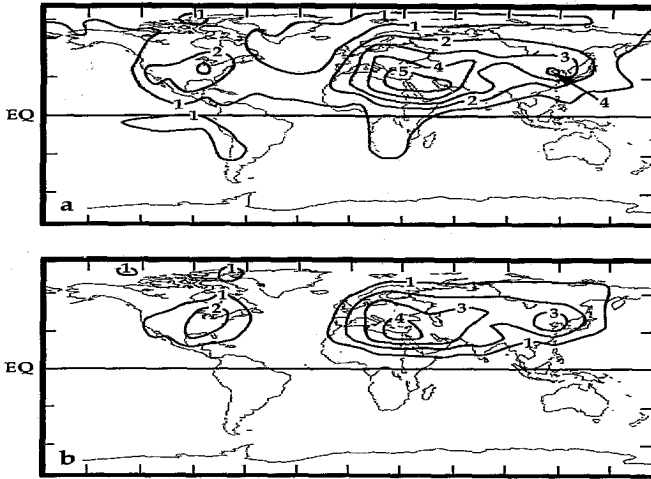


FIGURE 4: Global distribution of the reflected solar radiation due to tropospheric SO_4^{2-} ($\Delta F_R \text{ Wm}^{-2}$) for two scenarios: a) including anthropogenic and natural gaseous sulfur emissions, b) including only anthropogenic gaseous sulfur emissions.

sulfate aerosol burden therefore may have substantially countered, in the N.H., the expected climate warming due to the increase in concentrations of greenhouse gases. In addition, we would like to point out that the many fold increase in sulfate aerosol abundance over the polluted parts of the Eurasian and North America continents may have contributed to the radiation balance regionally so substantially that the temperature records of many stations may not be used to derive a possible “greenhouse warming” effect (37).

3.2. Indirect Forcing:

It is not possible to be as quantitative in comparing the direct effect with the possible indirect CCN effect of sulfate although, climate forcing due to CCN changes may also be important. Thus, although it seems evident that both chemical and meteorological factors are important in determining the CCN number concentration (38), no qualitative relationship is yet agreed upon. It appears likely that the CCN concentration may be a non-

linear function of the SO_4^{2-} aerosol particle mass concentration. The effect of CCN changes on cloud radiative properties was recognised first by Twomey (6), who drew attention to the potential influence of CCN on cloud albedo.

Concerning CCN from anthropogenic sources, in the N.H. the increased anthropogenic activities during the last century have strongly influenced the CCN concentrations. Wigley (39) for instance, has suggested that the slower warming of the N.H. compared to the S.H. could be explained by an increase of CCN of about 20% in the N.H. Ice core measurements performed by Neftel et al. (40) in Greenland have shown that in the N.H. non-sea-salt (nss) sulfate concentrations increased by a factor of 30%. Based on these results Schwartz (41) suggested that the present-day mean NH perturbation in cloud radiative forcing due to anthropogenic sulfates is approximately -2.0 Wm^{-2} . Substantially greater perturbations, -10.0 Wm^{-2} , or more, would be expected in regions directly influenced by industrial emissions, where CCN number concentrations are commonly enhanced by a factor of 5 or more above the natural background. However, while there certainly is potential for the anthropogenic sulfates to have increased the CCN number concentration, there are as yet no data and there is no agreed-upon theory relating number concentration of CCN to mass concentration of sulfates.

Concerning CCN from marine sources, Nguyen et al. (42), Charlson et al. (43), and Bates et al. (44) suggested that oceanic dimethylsulfide (DMS) emissions from phytoplankton in surface waters of the oceans could be involved in a climatic control through a cloud albedo feedback mechanism (figure 5). An increase of DMS flux from the ocean (70% of the Earth's surface) should therefore have a large climatic effect. Indeed, DMS might be the main source of CCN over unpolluted oceanic areas, where CCN concentrations are much smaller than over continents and so more sensitive to CCN source variations. The evidence of such an effect has been provided by satellite observations on enhanced cloud reflectivity in the tracks of ship's exhaust (45). A change of 30% of CCN over the oceans, influencing only marine low clouds (stratus) is calculated to change the global-mean short-wave radiative forcing by -2.0 Wm^{-2} (43). Furthermore, the sea surface albedo is low so that the cloud albedo effect is maximum: a 15% increase in the fractional low cloud cover (from 25% to 29% of the oceans surface) or reflectance would result in a planetary albedo increase able to counterbalance the doubling CO_2 greenhouse forcing (46).

Up to now several simultaneous measurements of CN and DMS have been reported. Correlation between DMS fluxes and CN concentrations (44, 47) and short term covariations between CN and atmospheric DMS concentrations (48) have been pointed out, but the relationship between CN concentrations and CCN concentrations have not been clearly demonstrated yet, particularly at low supersaturations (0.2%) that are typical of marine stratiform clouds.

It is clearly important to refine calculations for indirect aerosol effect in order to establish a theory relating number concentration of CCN to mass concentration of sulfates with a goal of quantify the indirect effect.

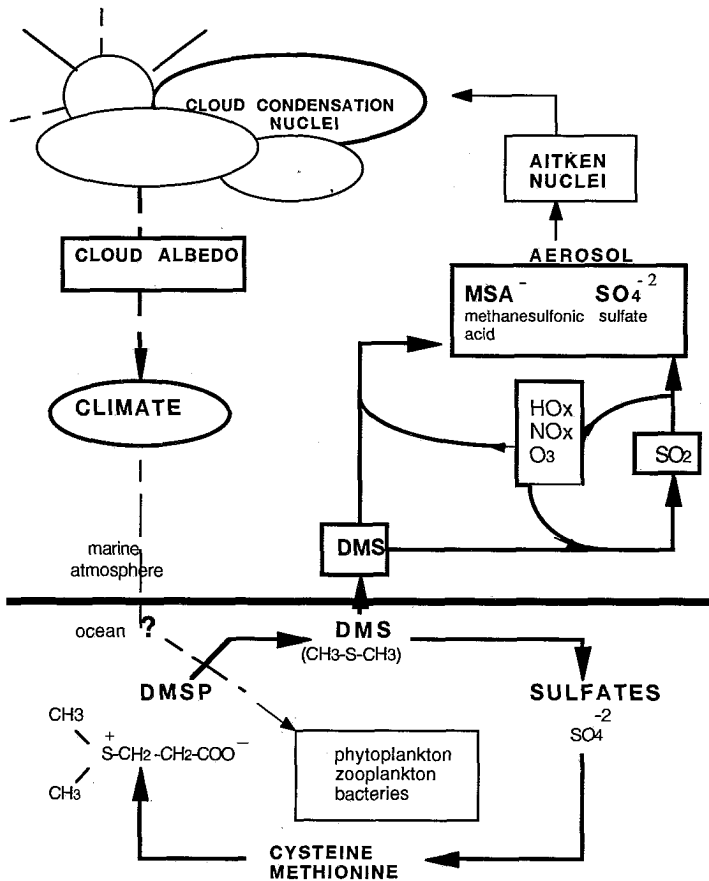


FIGURE 5. Possible interactions between oceanic DMS emissions and climate.

3.3. Future Changes

As we have seen it is presently very difficult to estimate with accuracy the "indirect" aerosol forcing. Thus every "future" scenario could be based only on the results presented in the "direct" aerosol forcing section. Another important point to consider is the different ways which sulfate and greenhouse gases can influence the radiative earth's budget. First of all sulfate has a very short atmospheric lifetime (of the order of week) compared with that of greenhouse gases which exceeds a decade. Thus high concentration of sulfates mainly occur near the emission zones (in the case of industrialised areas) and sulfate has only a regional rather than a global scale climate forcing. In addition, sulfate induced climate forcing has a distinctive diurnal and seasonal character being most intense during summer

(larger insolation) and of course, only during daylight hours, in contrast to the heat-trapping property of carbon dioxide which varies only moderately during the course of the day and through-out the year.

Thus any future changes in this forcing will depend on how the emissions of sulfate and greenhouse gases will vary. Because of the short atmospheric lifetime of sulfate and its precursors, the atmospheric burden will adjust within few weeks to changes in emissions. The situation is completely different for most greenhouse gases which have effective lifetimes of decades to centuries. For example, the concentration of CO_2 will continue to rise for more than a century even if emissions are kept constant at today's level. This difference is illustrated schematically in figure 6 (33), which shows how the climatic forcing due to CO_2 and aerosol sulfate would change if the global fossil fuel consumption levelled off and was eventually reduced.

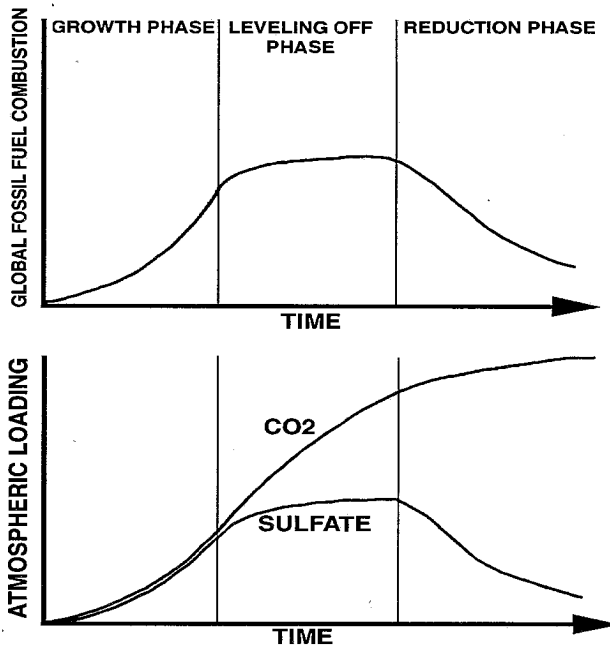


FIGURE 6: Illustration of the difference between response times of climate forcing due to CO_2 (heating) and sulfate (cooling) for different patterns of global fossil fuel consumption (from ref. 33)

Because of the rapid growth in emissions during the past decades both the greenhouse forcing due to CO_2 and the opposite forcing due to aerosol sulfate have grown accordingly. During a levelling off phase the greenhouse forcing will continue to grow whereas the

aerosol forcing will remain constant. During a decay phase, the greenhouse forcing due to CO_2 will start to level off and the aerosol cooling will decline. This simple example illustrates that the relative importance of these two major counteracting anthropogenic forcing agents in the future will depend critically on changes in the fossil fuel use (large scale desulfurization measures would of course also influence the sulfur emissions). Thus, the current tendency towards a balance in the N.H. is likely to change.

4. CONCLUSION AND PERSPECTIVES

The arguments and data presented above lead to the conclusion that both anthropogenic and natural sulfate produces a mean radiative climate forcing that is comparable in magnitude but opposite in sign to the anthropogenic perturbation in forcing by greenhouse gases. The direct aerosol and indirect cloud components each contribute a globally averaged forcing of roughly -1.0 Wm^{-2} to -2.0 Wm^{-2} .

However, aerosol forcing differs greatly in nature from greenhouse gas forcing. Such differences imply that aerosol influences have to be explicitly represented in future climate models rather than simply represented as a scaleable anti-greenhouse influence. In addition, the large uncertainties in the magnitude and geographical distribution of aerosol forcing, much larger than those associated with greenhouse forcing, indicate the need for substantial laboratory and field research both on global and local scales to improve the description of aerosol forcing. Among the components of such research program would be:

- Determination of the relative contributions of oceanic (DMS, DMSO, DMSO_2 , MSA, SO_4^{2-}) and continental (SO_2 , SO_4^{2-}) sources to the production of condensation nuclei (CN) and CCN,
- Determination of the relationship between aerosol size distribution, CCN concentration, droplet size distribution and cloud albedo,
- A new set of satellites dedicated to questions of radiative forcing and able to provide the needed global coverage and high frequency of sampling,
- Development of specific algorithms for satellite data analysis to allow the comparison of cloud albedo and cloud microphysical properties in various areas representing different CCN concentrations (oceans, polluted continents),
- Modelling of the influence of various sulfur atmospheric concentrations to the CCN population.

ΠΕΡΙΛΗΨΗ

Το ενεργειακό ισοζύγιο της γης επηρεάζεται από την ύπαρξη αερίων σε ιχνη και αιωρούμενων σωματιδίων στην ατμόσφαιρα. Τα ιχνοαέρια που επηρεάζουν θετικά το ενεργειακό ισοζύγιο (φαινόμενο του θερμοκηπίου) μπορούν να συμμετασχουν είτε άμεσα (π.χ. CO_2 , CH_4 , CFCs, N_2O , O_3) είτε έμμεσα μεταβάλλοντας την οξειδωτική

κατασταση της ατμοσφαιρας (π.χ. CO, μη μεθανικοι υδρογονανθρακες). Τα αιωρουμενα σωματιδια μπορουν επισης να επηρεασουν το ενεργειακο ισοζυγιο της γης ειτε αμεσα (διαχυση του προσπιπτωντος ηλιακου φωτος) ειτε εμμεσα (μεταβαλλοντας τον αριθμο των πυρηνων συμπυκνωσης και κατα συνεπεια την διαθλαστικοτητα των συννεφων). Εντουτοις η υπαρξη τους οδηγει σε αντιθετα αποτελεσματα (μειωση της θερμοκρασιας της ατμοσφαιρας). Ετσι προσφατες εκτιμησεις που πραγματοποιηθηκαν με την βοηθεια μοντελων 3-διαστασεων εδειξαν οτι τα θεικα ιοντα των αιωρουμενων σωματιδιων μπορουσαν να προκαλεσουν μια μειωση της ενεργειας που δεχεται η γη απο τον ηλιο της ταξης του 1.5 με 2.5 W/m². Το μεγεθος αυτο ειναι συγκρισιμο (αλλα αντιθετου φορας) με την αναμενομενη αυξηση λογω του CO₂.

Το SO₂ που προερχεται απο την καυση των ορυκτων καυσιμων και το θειουχο διμεθυλιο (DMS) που εκπεμπεται απο το θαλασσιο φυτοπλαγκτον της ευφωτης ζωνης και το οποιο οξειδωνεται στην ατμοσφαιρα σε μεθανοσυλφονικο οξυ (MSA) και θεικα ιοντα αποτελουν τις κυριότερες πηγες ανθρωπογενους και βιογενους προελευσης σωματιδιων στην ηπειρωτικη και θαλασσια ατμοσφαιρα. Στο παρον αρθρο παρουσιαζουμε μια ανασκοπηση των πηγων εκπομπης του θειου στην ατμοσφαιρα, της χημειας του (στην ατμοσφαιρα) καθως και του πιθανου κλιματικου του ρολου.

Acknowledgments. Useful comments on the manuscript by Dr. I. Barnes are gratefully acknowledged. This work was supported by a french-greek collaboration (program PLATON).

REFERENCES

1. Intergovernmental Panel on Climate Change (IPCC), The IPCC Scientific Assessment, J.T., Houghton, G.T.J. Jenkins, J.T. Ephraums, Eds. Cambridge Univ. Press, Cambridge, 1990.
2. Angstrom, A., On the atmospheric transmission of sun radiation and on dust in the air. *Geografiska. Annaller* 11, 156-159, 1929.
3. Coacley, J.A.Jr., Cess, R.D., and Yurevich, F.B., The effect of tropospheric aerosols on the earth's radiation budget: a parameterisation for climate models, *J. Atmos. Sci.* 40, 116-138, 1983.
4. Simoneit, B.R.T., and Mazurek, M.A., "Organic matter on the troposphere. II. Natural background of biogenic lipid matter in aerosols over the rural western United States, *Atmos. Environ.* 16, 2139, 1982.
5. Ackerman, T.P., and Toon, O.B., Absorption of visible radiation in atmosphere containing mixtures of absorbing and nonabsorbing particles, *Applied Optics*, 20, 3661-3667, 1991.
6. Fouquart, Y., marine aerosol particles, CCNs clouds and climate, report to WCRP/JSC,

Bremen, March 1993.

7. Nguyen, B.C., Belviso, S., Mihalopoulos, N., Gostan, J., and Nival, P., Dimethylsulfide production during natural phytoplanktonic blooms, *Marine Chem.*, 24, 133-141, 1988.
8. Moller, D., Estimation of the global man-made sulphur emission, *Atmos. Environ.* 18, 19-27, 1984.
9. Hameed, S., and Dignon, J., Changes in the geographical distributions of global emissions of NO_x and SO_x from fossil fuel combustion between 1966 and 1980, *Atmos. Environ.* 22, 441-449, 1988.
10. Semb, A., Circumpolar SO₂ emission survey, NILU OR69/85, Norwegian Institute for Air Research, Lillestrom, Norway, 1985.
11. Hao, W., Liu, M.H., and Crutzen, P.J., Estimates of annual and regional releases of CO₂ and other trace gases to the atmosphere from fires in the tropics, based on the FAO statistics for the period 1975-1980. In: *Fire in the tropical biota*, J.G. Goldammer, Ed. (Springer-Verlag, Berlin), 440-462, 1991.
12. Andreae, M.O., et al., Biomass burning and associated haze layers over Amazonia. *J. Geophys. Res.* 93, 1509-1527, 1988.
13. Bates, T.S., et al., Regional and seasonal variations in the flux of oceanic dimethylsulfide to the atmosphere, *J. Geophys. Res.* 92, 2930-2938, 1987.
14. Leck, C., and Rodhe, H., Emissions of marine biogenic sulfur to the atmosphere of Northern Europe, *J. Atmos. Chem.* 12, 63-86, 1991.
15. Berresheim H., and Jaeschke, W., The contribution of volcanoes to the global atmospheric sulphur budget, *J. Geophys. Res.* 88, 3732-3740, 1983.
16. Goldan, P.D., et al., The measurement of sulfur emissions from soils and vegetation: Three sites in the eastern United states revised, *J. Atmos. Chem.* 5, 429-437, 1987.
17. Lamb, B., et al., Measurement of biogenic sulfur emissions from soils and vegetation: Application of dynamic enclosure methods with Natusch filter and GC/FPD analysis, *J. Atmos. Chem.* 5, 469-491, 1987.
18. Andreae, M.O., and Andreae, T.W., The cycle of biogenic sulfur compounds over the Amazon Basin, 1. Dry season, *J. Geophys. Res.* 93, 1487-1497, 1988.
19. Plane, J.M., Gas phase atmospheric oxidation of biogenic sulfur compounds: A review, in *Biogenic sulfur in the Environment*, E.S. Saltzman and W.J. Cooper Eds, Washington, DC, 404-423, 1989.
20. Mihalopoulos, N., et al., Field study of dimethyl sulfide oxidation in the boundary layer: variations of dimethylsulfide, methanesulfonic acid, sulfur dioxide, non-sea-salt sulfate and Aitken nuclei at a coastal site, *J. Atmos. Chem.* 14, 459-477, 1992.
21. Putaud, J.P., et al., Seasonal variations of atmospheric sulfur dioxide and dimethylsulfide concentrations at Amsterdam island in the southern Indian Ocean, *J. Atmos. Chem.* 15, 117-133, 1992.
22. Yin, F., Grosjean D., Seinfeld J.H., Photooxidation of dimethyl sulfide and dimethyl

- disulfide. I: Mechanism development, *J. Atmos. Chem.*, 11, 309-364, 1990.
23. Barnes, I., Bastian, V., and Becker, K.H., Kinetics and Mechanisms of the reactions of OH radicals with dimethyl sulfide, *Int. J. Chem. Kinet.* 20, 415-431, 1988.
24. Mihalopoulos, N., Putaud, J.P., and Nguyen, B.C., Seasonal variation of methanesulfonic acid in precipitation at Amsterdam island in the southern Indian Ocean, *Atmos. Environ.*, 27, 2069-2073, 1993.
25. Saltzman, E.S., et al., Methanesulfonic acid and non-sea-salt sulfate in Pacific air: regional and seasonal variations, *J. Atmos. Chem.* 4, 227-240, 1986.
26. Berresheim, H., Biogenic sulfur emissions from the Subantarctic and Antarctic oceans, *J. Geophys. Res.*, 92, 13245-13262, 1987.
27. Barnes, I., Becker, K.H., and Patruescu, I., The tropospheric oxidation of dimethyl sulfide: A new source of carbonyl sulfide, *J. Geophys. Res. Lett.*, 21, 2389-2392, 1994.
28. Calvert, J.G., et al., Chemical mechanisms of acid generation in the troposphere, *Nature*, 317, 27-35, 1985.
29. Penkett, S.A., et al., The importance of atmospheric ozone and hydrogen peroxide in oxidizing sulfur dioxide in cloud and rainwater, *Atmos. Environ.* 13, 123-145, 1979.
30. Martin, L.R., Kinetic studies of sulfite oxidation in aqueous solutions, in SO₂, NO, and NO₂ oxidation mechanisms: Atmospheric consideration, Acid precipitation series, J.I. Teasley, Series Ed., Butterworth, Boston, 1984, pp. 63-100 and references therein.
31. Langner, J., and Rodhe, H., A global three-dimensional model of tropospheric sulphur cycle, *J. Atmos. Chem.*, 13, 225-245, 1991.
32. Charlson, R.J., et al., Climate forcing by anthropogenic aerosols, *Science*, 423-430, 1992
33. Charlson, R.J., et al., Perturbation of the northern hemisphere radiation balance by backscattering from anthropogenic sulfate aerosols, *Tellus*, 43AB, 152-163, 1991
34. Zimmermann, P.H., Ein dreidimensionales numerisches transportmodell fuer atmosphärische spuerenstoffe, Ph. D. Dissertation, University of Mainz, Germany, 1984.
35. Zimmermann, P.H., A handy global tracer model. In: Proceedings of the 16th NATO/CCMS International Technical Meeting on Air Pollution Modeling and its Application, Lindau, Germany, Reidel, Dordrecht, 593-608, 1987.
36. Feichter, J., and Crutzen, P.J., Parameterization of deep cumulus convection in a global tracer transport model, and its evaluation with 222Rn, *Tellus*, 42B, 110-117, 1990.
37. Crutzen, P.J., and Lelieveld, J., Submitted to *Nature*.
38. Baker, M.B., and Charlson, R.J., Bistability of CCN concentrations and thermodynamics in the cloud-topped boundary layer, *Nature*, 345, 142-145, 1990.
39. Wigley, T.M. L., Possible climate change due to SO₂ derived cloud condensation nuclei, *Nature*, 339, 365-367, 1989
40. Nefel, A., et al., Sulphate and nitrate concentrations in snow from South Greenland, *Nature*, 314, 611-613, 1985.
41. Schwartz, S.E., are global cloud albedo and climate controlled by marine

phytoplankton? *Nature*, 336, 441-445, 1988.

42. Nguyen, B.C., Bonsang, B., and Gaudry, A., the role of the ocean in the global atmospheric sulfur cycle, *J. Geophys. Res.*, 88, 10903-10914, 1983.

43. Charlson, R.J., et al., Oceanic phytoplankton, atmospheric sulphur, cloud albedo and climate, *Nature* 326, 655-661, 1987.

44. Bates, T.M., Charlson, R.J. and Gammon, R.H., Evidence for the climate role of marine biogenic sulphur, *Nature*, 329, 319-321, 1987.

45. Coacley, J.A., Jr., Bernstein, R.L., and Durkee, P.A., effect of ship-stack effluents on cloud reflectivity, *Science*, 237, 1020-1022, 1987.

46. Albrecht, B.A., Aerosols, cloud microphysics and fractional cloudiness, *Science*, 245, 1227-1230, 1989.

47. Ayers, G.P., Ivey, J.P., and Gillett, R.W., Coherence between seasonal cycles of dimethylsulfide, methanesulfonate, and sulphate in marine air, *Nature*, 349, 404-406, 1991.

48. Putaud J.P., et al., Dimethylsulfide, aerosols and condensation nuclei over the tropical northeastern Atlantic Ocean, *J. Geophys. Res.*, 98, 14863-14871, 1993.

MIKTOARM STAR POLYMERS

N.HADJICHRISTIDIS*, H.IATROU, Y.TSELIKAS, V.EFSTRATIADIS
University of Athens, Department of Chemistry,
Panepistimiopolis, Zografou, 157 71 Athens, Greece.

Received: July 8, 1995

SUMMARY

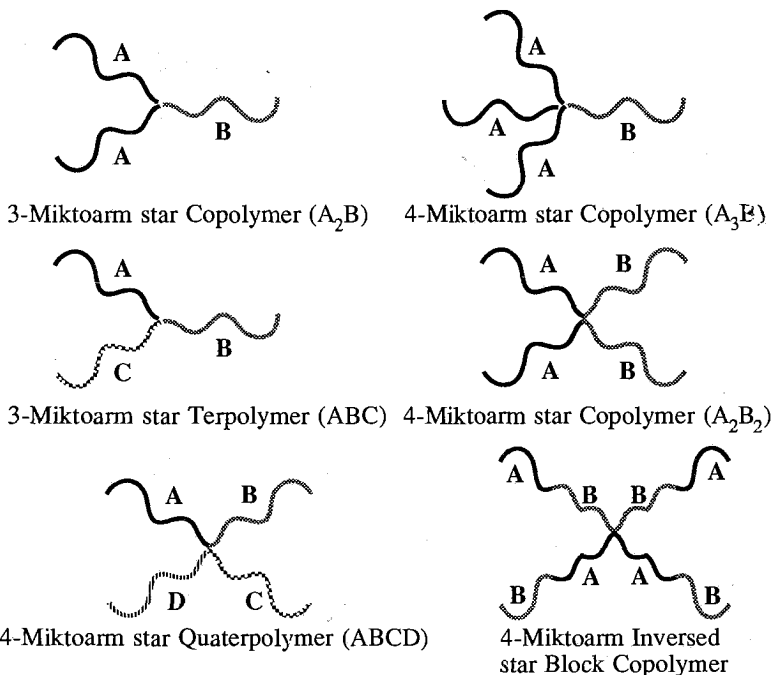
The synthetic routes leading to star polymers with chemically different arms, the so-called miktoarm stars, are being reviewed. Most of the methods are based on anionic polymerization techniques and the use of appropriate linking agents as divinylbenzenes, double 1,1-diphenylethylenes or chlorosilanes. Due to the fact that these polymers have been prepared recently, only limiting results exist for dilute solution and bulk properties. Nevertheless, it seems that these materials will open new horizons in polymer science and technology.

KEY WORDS: Miktoarm star polymers, anionic polymerization, divinylbenzenes, double 1,1-diphenylethylenes, chlorosilanes, dilute solution properties, morphology, rheology

INTRODUCTION

Star polymers are branched species with one single branch point from which emanate a number of arms. Miktoarm (mikto from the greek word $\mu\kappa\tau\acute{o}\varsigma$ meaning mixed) are star polymers with chemically different arms (Scheme 1). Due to the fact that model miktoarm star polymers have been prepared only recently, this review will mainly focus on the synthesis of these new materials. Emphasis will be given to the miktoarm star polymers prepared at the University of Athens. The limited results existing on the properties and potential applications of these polymers will also be given.

Scheme 1
A few examples of Miktoarm Star Polymers



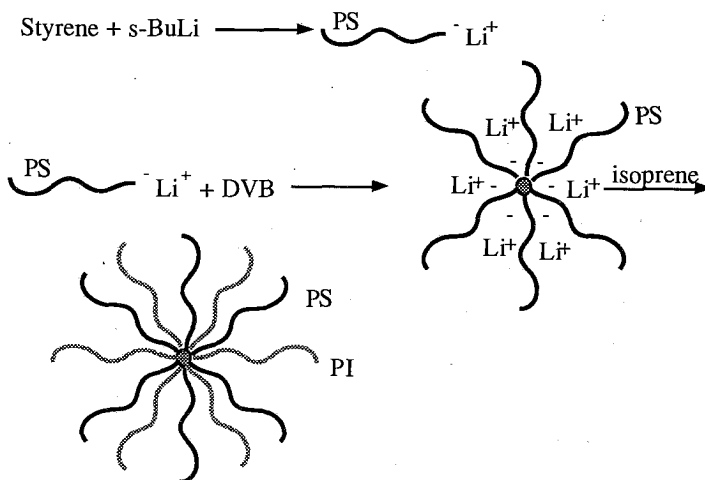
STRATEGIES AND METHODS FOR PREPERATION

Although there are several individual methods for the synthesis of miktoarm stars, three general methodologies have been developed, based on anionic polymerization techniques and the use of appropriate linking agents.

A. Divinylbenzene Approach

In this approach, the polymerization of a small amount of divinyl benzene (DVB), usually a mixture of the three isomers, is initiated by the living ends of the polymeric chains. This leads to the formation of star molecules, which are constituted of a poly(divinylbenzene) (PDVB) core connected to a number of polymeric chains. The core contains the same number of anionic sites as the number of arms. These "living" star polymers may then be used to initiate the polymerization of another

monomer, creating new branches growing out from the core. Eschwey and Buchard (1) were the first to publish, the synthesis of "mixed" stars of styrene and isoprene, by using this strategy, according to the following reaction scheme:



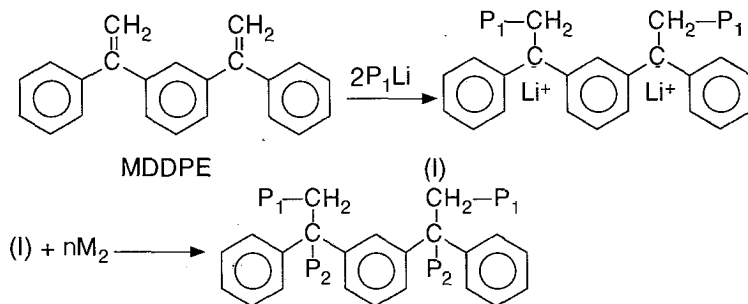
(mixed star of styrene and isoprene)

Rempp et al.(2,3), using the same approach have prepared miktoarm star copolymers of the A_nB_n type, where A is polystyrene and B is poly(tert-butyl methacrylate), poly(n-butyl methacrylate), or poly(tert-butyl acrylate).

This method suffers the disadvantage of architectural limitations, since it is possible to prepare miktoarm stars only of the A_nB_n structure. Moreover, it is difficult to control precisely the number of arms, because the linking reaction is a random procedure. As a consequence, the resulting copolymers present polydispersity in the number of arms. In addition the weight of the PDVB core can represent a large percentage of the total weight of the star, altering the properties of the material.

B. Double 1,1-Diphenylethylenes Approach.

This approach based on the work of Szwarc and collaborators(4) involves the reaction of living polymeric chains with double 1,1-diphenylethylenes as linking agents, as f.e. 1,3-di(1-phenylethenyl) benzene or meta double 1,1-diphenylethylene (MDDPE). A second monomer is added to the living coupled product, and a miktoarm star of the A_2B_2 type is formed. The general reaction scheme is as follows:



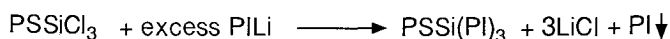
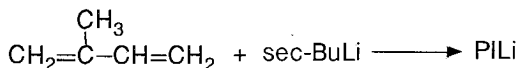
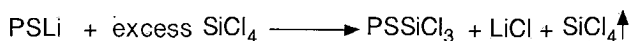
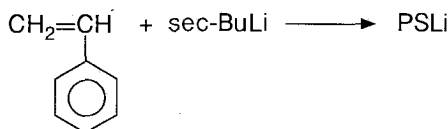
Quirk et al (5), using this approach, have prepared 4-miktoarm star copolymers of the A₂B₂ type where A is polystyrene and B is polyisoprene or polybutadiene. Also by using a different isomer they were able to prepare 3-miktoarm star homopolymers (different arm lengths) and copolymers of the A₂B and ABC type, where A,B,C are polystyrene (PS), polyisoprene (PI) or polybutadiene (PBd).

One of the weak points of this method is the different reaction rate of the first and the second living polymeric chain with the monomer M₂ in hydrocarbon solvents. As a consequence, the two propagating chains have different length. In order to avoid this problem polar additives were used, but these increase the vinyl content of the polydienes grown from the active centers, if the second monomer is a diene. As in the case of the DVB approach, it is difficult to extend this method to more complicated structures such as AB₅, A₂B₄, ABCD e.t.c.

C. Chlorosilane Approach.

In 1988 Pennisi and Fetters (6), based on the work of Morton and collaborators(7), prepared model three-arm asymmetric PS and PBd homopolymer stars of the A₂B type, where two arms have equal length and the third arm was longer or shorter. The synthetic approach involves the reaction of living arm B with an excess of methyltrichlorosilane, followed, after the removal of the excess of the linking agent, by the addition of a slight excess of the living arm A. After linking is completed, the residual linear A chains are removed by fractionation.

Mays (8) employed this approach to prepare a nearly monodisperse 3-miktoarm star copolymer of the A₂B type, where A is PI and B is PS. The same method was applied by Hadjichristidis and collaborators for the synthesis of almost all combinations of PS with PI and PBd in the case of A₂B type stars(9) and for the synthesis of A₃B type stars where B is PS and A is PI(10). The basic reactions, for example, used for the synthesis of the 4-miktoarm star copolymers of the A₃B type, are the following:



The excess of PILi after neutralization with methanol is removed by fractionation. For the synthesis of the A₂B stars, CH₃SiCl₃ is used instead of SiCl₄.

In Table 1 the molecular characteristics of a few A₂B and A₃B miktoarm star copolymers are given. It is clear that these copolymers are model compounds having a high molecular and compositional homogeneity. This fact is also supported by the excellent agreement between the composition of the miktoarm copolymers calculated from the M_n of the arms and the ones found by UV and NMR.

Table 1
Molecular characteristics of 3- and 4- miktoarm star copolymers of the A₂B and A₃B type

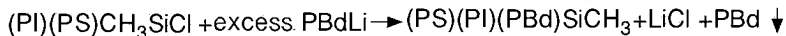
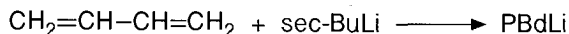
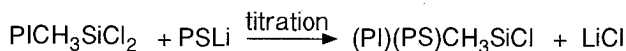
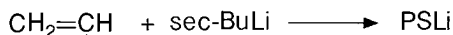
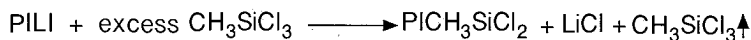
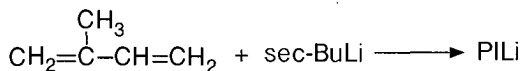
Sample	M _n x10 ⁻³			M _w x10 ⁻³	I
	PS	PDiene	Star	Star	Star
PS(PI) ₂	21.7	19.9	50.3	53.4	1.05
(PS) ₂ PI	20.8	33.8	70.4	75.3	1.05
PS(PBd) ₂	21.7	9.5	34.7	41.1	1.05
(PS) ₂ PBd	13.0	22.0	44.4	47.8	1.05
PS(PI) ₃	35.2	14.5	77.2	80.1	1.05
PS(PI) ₃	180	7.6	199	204	1.03

I=M_w/M_n. Polydispersity index.

The chlorosilane method was extended by Iatrou and Hadjichristidis for the synthesis of 3- miktoarm star terpolymers of the ABC type and of 4-miktoarm star co- and quaterpolymers of the A₂B₂ and ABCD types(11,12).

For the 3-miktoarm star terpolymer (Scheme 1) the synthetic approach involved the reaction of poly(isoprenyllithium) with an excess of methyltrichlorosilane, followed after removal of the excess of the linking

agent, by a stoichiometric addition (titration) of PSLi, and finally by the addition of a small excess of PBLi. The basic reactions used are the following:



The synthesis of the star terpolymer relies, on one hand, on the inability, under the experimental conditions employed, of the sterically hindered polystyryl anion to undergo complete reaction with the macromolecular difunctional linking agent, and on the other hand, on the ability of the less sterically hindered polybutadienyl anion to react completely with the monofunctional macromolecular linking agent. Thus the sequence of the addition of the living polymers is very critical. The synthesis was monitored via size exclusion chromatography (SEC). SEC chromatograms of the precursors along with the ones taken during the synthesis and those of the raw product and of the fractionated 3-miktoarm star terpolymer are shown in Figure 1. The characteristics of the precursors and the fractionated terpolymers given in Table 2 indicate the high molecular and compositional homogeneity of this sample. In addition, the PS content calculated by the arms molecular weight and that found by UV and NMR are in excellent agreement.

Table 2

Molecular characteristics of 3-miktoarm star terpolymers of the ABC type

Sample	$M_n \times 10^{-3}$				$M_w \times 10^{-3}$	I
	PS	PI	PBd	Star	Star	
ABC1	20.7	15.6	12.2	45.4	46.4	1.04
ABC2	7.9	8.2	7.7	23.8	24.7	1.04

$I = M_w/M_n$. Polydispersity index.

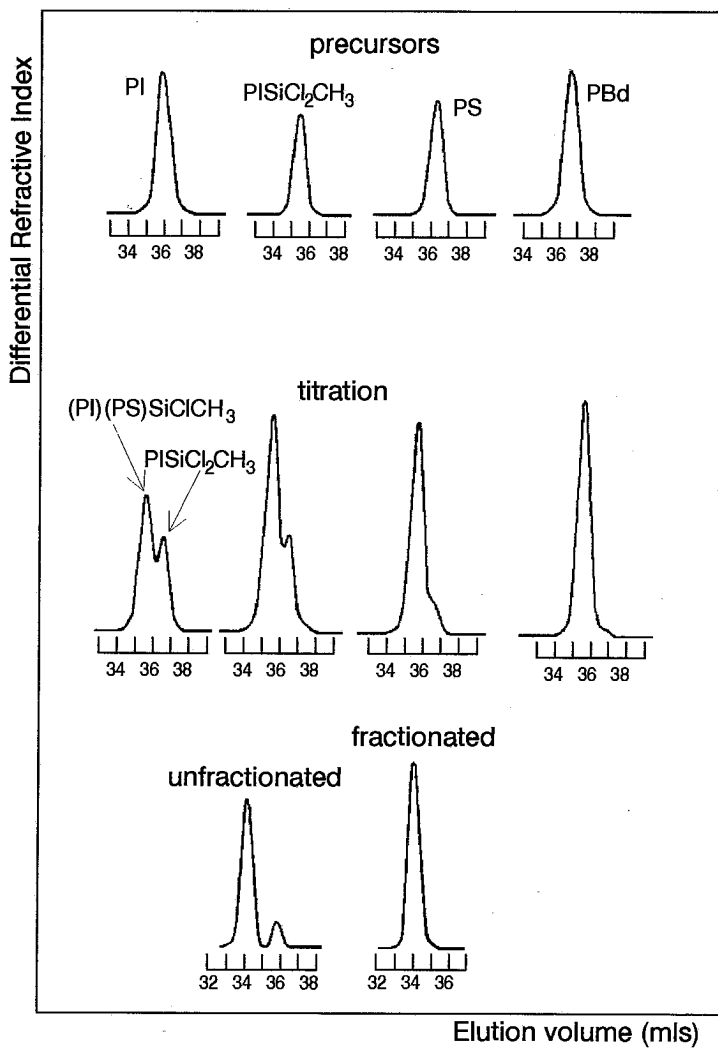
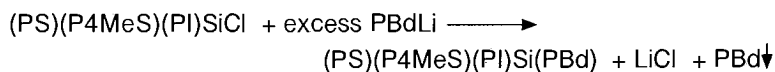
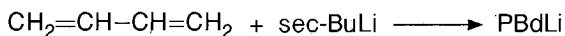
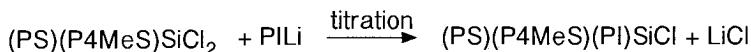
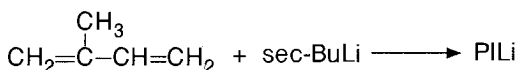
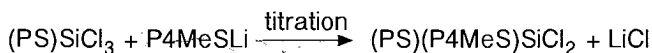
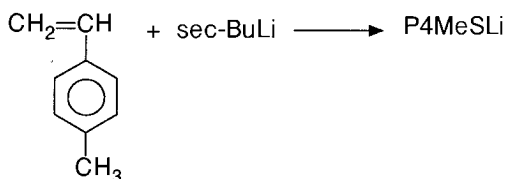
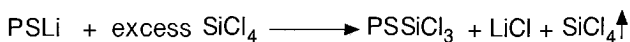
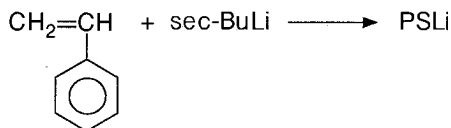


Figure 1

SEC chromatograms taken during the different stages of the synthesis of the ABC miktoarm star terpolymer

Following a procedure similar to that used for the ABC the synthesis of the 4-miktoarm star copolymer of the A_2B_2 type (Scheme 1), where A is PS and B is PBd was accomplished. The PSLi was added in two separate steps (excess and titration) in order to have the maximum control in the incorporation of the second arm. The molecular characteristics of the fractionated copolymer indicated a high degree of molecular and compositional homogeneity (model polymer).

In the case of the ABCD 4-miktoarm star quaterpolymer (Scheme 1), a similar strategy was used according to the following reaction scheme:



As in the case of the ABC 3-miktoarm star, the order of addition of the arms to the linking agent is important. So the sterically hindered polystyryl anion is the first arm to be added to an excess of SiCl_4 . After removal of the excess of SiCl_4 the even more sterically hindered poly(4-methylstyryl) anion can be successfully titrated as the second arm, so that only one arm can be incorporated in the star. The moderately hindered polyisoprenyl anion is best suited for titration as the third arm, while the

less sterically hindered polybutadienyl anion is the only one able to react completely with the sterically hindered monofunctional macromolecular linking agent, and therefore it is the last to be added. The molecular characteristics of this quaterpolymer shown in Table 3 indicate the success of the synthetic approach.

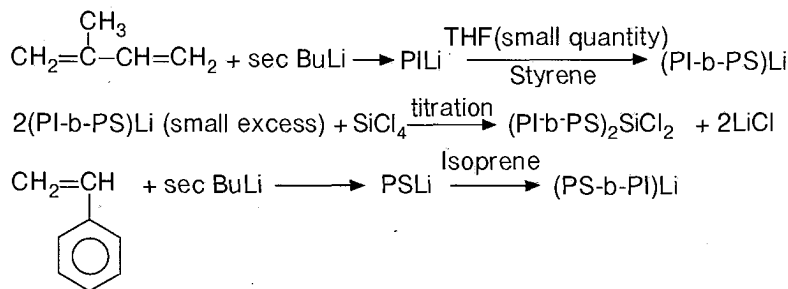
Table 3
Molecular characteristics of the 4- miktoarm star quaterpolymer of the ABCD type

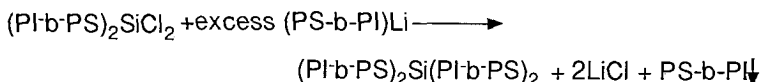
Sample	$M_n \times 10^{-3}$					$M_w \times 10^{-3}$	I
	PS	PI	PBd	P4MeS	Star	Star	Star
(PS)(P4MeS)(PI)(PBd)	15.9	14.5	16.2	15.4	62.5	65.5	1.06

$I = M_w/M_n$. Polydispersity index.

As mentioned above, the successful synthesis of miktoarm star polymers relies on the differences in steric hindrance between the living precursors of the different arms of the star. A key factor in the synthesis, is the participation of at least one sterically hindered polystyryl anion, which allows the controlled addition of a certain number of arms (1 or 2). In order to synthesize miktoarm star copolymers without polystyrene arms one has to make some modifications in the conventional chlorosilane route. Two strategies⁽¹³⁾ have been reported for the synthesis of a series of A₂B₂ miktoarm stars, A being polyisoprene and B being polybutadiene. The first involves capping of the polyisoprenyllithium chains, with 2-3 units of styrene in order to increase the steric hindrance, followed by titration with SiCl₄ and reaction with an excess of polybutadienyllithium. The second method carries out the linking reaction of the first two arms at -40°C, in order to lower the overall reactivity of the living polydiene towards the reaction with the chlorosilane, followed by addition of an excess of polybutadienyllithium.

Another type of miktoarm stars prepared using the chlorosilane approach is the inversed starblock miktoarm copolymer (Scheme 1). The basic reactions for its synthesis are the following:⁽¹⁴⁾





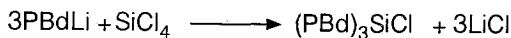
During the synthesis of the (PI-b-PS)Li living diblock, a small amount of THF was added in order to increase the reactivity of the polyisoprenyllithium anion towards styrene initiation. Thus the styrene polymerization has a fast initiation step and the narrow distribution of the (PI-b-PS)Li arm is ensured. The titration step was monitored by SEC. The molecular characteristics of the inverse starblocks (ISB) given in Table 4 indicate a high degree of homogeneity.

Table 4
Molecular characteristics of inverse starblock copolymers

Sample		SB1	SB2	SB3
Mn(PS) x 10 ⁻³		82.0	36.1	20.0
Mn(PS-b-PI) x 10 ⁻³		101	52.6	37.3
%wt PS Content	UV-SEC	80	65	49
	¹ H NMR	80	68	48
Mn(PI) x 10 ⁻³		73.0	32.5	17.9
Mn(PI-b-PS) x 10 ⁻³		93.1	50.0	37.4
%wt PS Content	UV-SEC	20	35	50
	¹ H NMR	21	37	51
Mn(star) x 10 ⁻³		378	212	148
Mw(star) x 10 ⁻³		395	220	152
I(star) (SEC)		1.05	1.04	1.03
%wt PS Content	UV-SEC	48	50	49
	¹ H NMR	50	49	49
	dn/dc	53	51	51
	calculated	50	51	50

I=M_w/M_n. Polydispersity index.

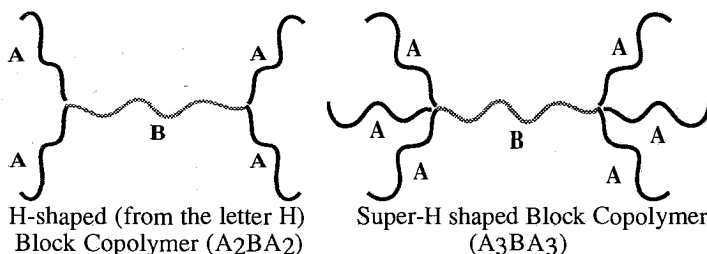
By using the chlorosilane approach Tsiang⁽¹⁵⁾ has prepared miktoarm stars of the (AB)₃ type where B is PB and A is PS. His approach involves the reaction of SiCl₄ with three equimolar amounts of living arm B, followed by the addition of the living diblock copolymer, according to the following reactions:



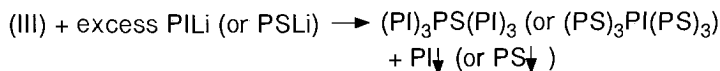
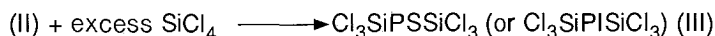
The weak point of the method is that in the first linking step, besides the main product ClSiB_3 , there are also SiB_4 , Cl_2SiB_2 and BSiCl_3 produced. The last two side products, after the second linking step, will be transformed to $(\text{AB})_2\text{SiB}_2$ and $\text{BSi}(\text{AB})_3$ respectively, and it is very difficult to separate them from the $(\text{AB})_3\text{SiB}_3$.

The chlorosilane approach, properly used can lead not only to other miktoarm stars [for example $(\text{AB})_2\text{A}_2$, $(\text{AB})_2\text{B}_2$, $(\text{AB})_2\text{BC}$, AB_5 , $(\text{AB})\text{B}_5$, $(\text{AB})\text{A}_5$ etc] but also to more complicated architectures (Scheme 2).

Scheme 2
H-Shaped and Super-H shaped block copolymers



For the synthesis of the A_3BA_3 type the following reactions were used by Hadjichristidis and collaborators⁽¹⁶⁾:



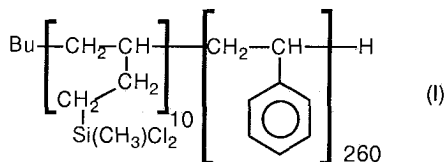
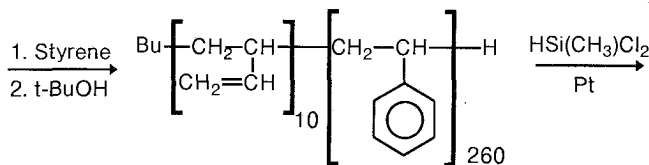
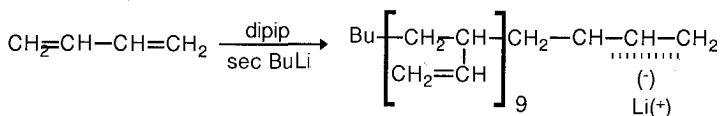
The living difunctional polymer, prepared by the procedure described by Roovers and Toporowski⁽¹⁷⁾, is added to a very large excess of SiCl_4 to obtain the bridging polymer chain (or connector) functionalized at both ends with the $-\text{SiCl}_3$ group. Addition of an excess of living polymer of the branches leads to the super-H copolymer. The H-shaped copolymer is obtained by using CH_3SiCl_3 instead of SiCl_4 . The molecular characteristics (Table 5) indicate a high degree of molecular and compositional homogeneity.

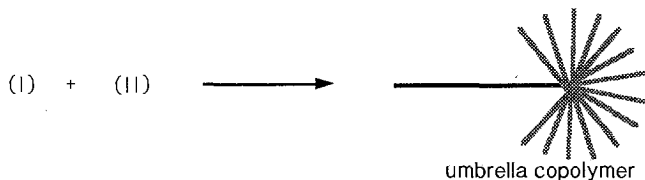
Table 5
Molecular Characteristics of the Super-H Shaped Block Copolymers

Sample	Mn x 10 ⁻⁴			Mw x 10 ⁻⁴	I	%wt PS-d8	
	PS-d8	PI	SH	SH	SH	Mn	UV
SH 10-20	0.84	1.56	10.8	10.9	1.04	8.2	8.5
SH 10-10	0.84	1.03	6.87	7.13	1.04	11.5	12
SH 20-20	1.68	1.79	12.0	12.8	1.03	13.5	14
SH 40-20	4.59	1.56	14.1	14.9	1.03	33	33
SH 40-10	4.59	1.03	10.6	11.4	1.04	43	42
SH 80-10	8.46	1.03	15.1	15.4	1.03	58	57

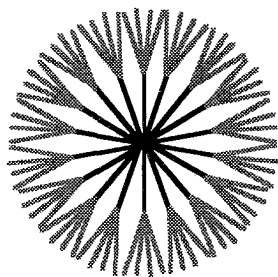
I=M_w/M_n. Polydispersity index; PS-d8: deuterated PS.

Wang and Roovers⁽¹⁸⁾ using the chlorosilane approach have prepared umbrella copolymers of the AB_n type and umbrella star copolymers of the general (AB_n)_m type where A is PS and B is PBd or poly(2-vinyl pyridine) (P2VP). The approach involves polymerization of butadiene in the presence of dipiperidinoethane (dipip) followed by styrene addition. A PS chain having at the end a short 1,2-PBd chain is produced. The functional groups -Si(CH₃)Cl₂ or -Si(CH₃)₂Cl were then inserted to the 1,2 PBb vinyl double bonds by using chlorosilylation chemistry. Finally addition of PBd(1,4)Li or P2VPK produce the umbrella type copolymer. The reaction scheme for the case of PS(PBd)_n type umbrella copolymer is given below:





The procedure for the umbrella star copolymers is similar to the one mentioned above. The difference is that the living (PBd_{1,2})PSLi precursor was reacted with an appropriate linking agent to produce a star shaped copolymer which after hydrosilylation is converted to a dendritic coupling agent. Reaction with PBd(1,4)Li or PV2PK leads to the following architecture:



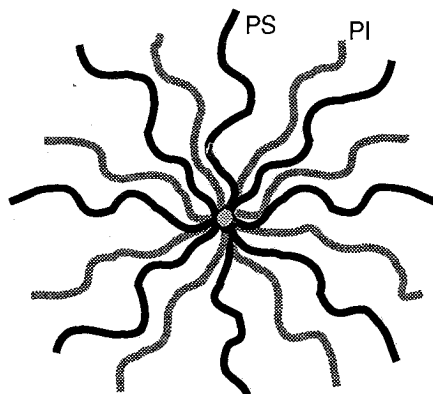
umbrella star copolymer

The only disadvantage of this method is that since the hydrosilylation reaction is not complete, the control over the number of arms is very difficult.

Hadjichristidis and collaborators, by using the chlorosilane approach, have prepared miktoarm star copolymers of the (PS)₈(PI)₈ type⁽¹⁹⁾, the so called "Vergina Star Copolymers" (Scheme 3) named from the similarity to the 16-rayed star discovered by Professor M. Andronikos of the University of Thessaloniki, in the ancient tomb of Philip of Macedonia in Vergina, a place close to Thessaloniki.

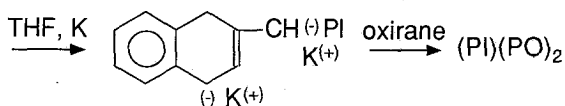
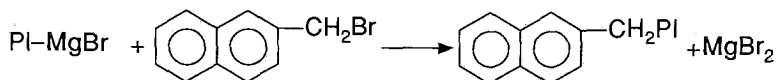
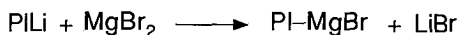
$\text{Si}[\text{CH}_2\text{CH}_2\text{Si}(\text{CH}_3)(\text{CH}_2\text{CH}_2\text{Si}(\text{CH}_3)\text{Cl}_2)_2]_4$ which is a silane having 16 chlorine atoms, was used as the linking agent. In the first step of the synthesis butadiene-capped "living" polystyrene was added to the linking agent in a stoichiometric ratio of 8/1, in order to accomplish the incorporation of 8 polystyrene arms in the molecule. After the completion of this reaction an excess of polyisoprenyllithium was added to obtain the "Vergina" star copolymer.

Scheme 3
Vergina Star Copolymer

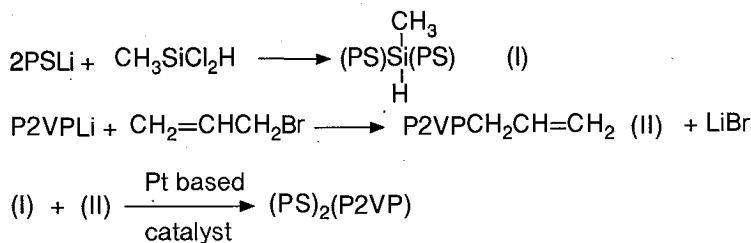


D. Individual Methodologies.

Teysse and coworkers (20) by using naphthalene terminated polymers have prepared miktoarm star copolymers of the A₂B type, where A is polyoxirane (PO) and B is polystyrene (PS) or poly (*p*-tert-butylstyrene) (PTBS) or polyisoprene (PI) according to the reactions:

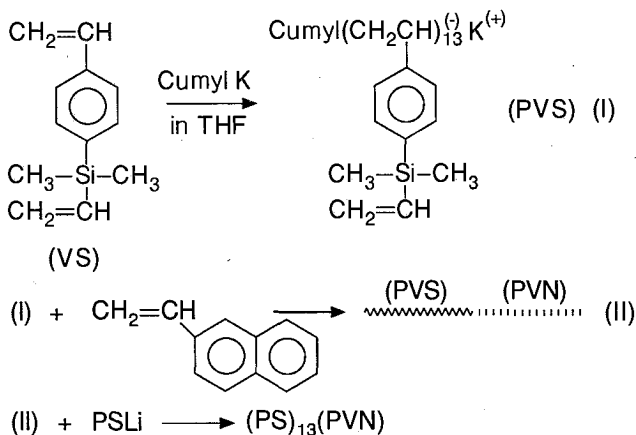


Khan et al.(21) using anionic polymerization techniques and CH₃SiCl₂H as linking agent have prepared 3-miktoarm star copolymers of the A₂B type, where A is polystyrene (PS) and B poly (2-vinylpyridine) (P2VP) according to the following general reactions:



This approach generally gives polymers with polydispersity as high as 1.5, maybe due to the incomplete hydrosilylation, especially in the case of the higher molecular weight arms.

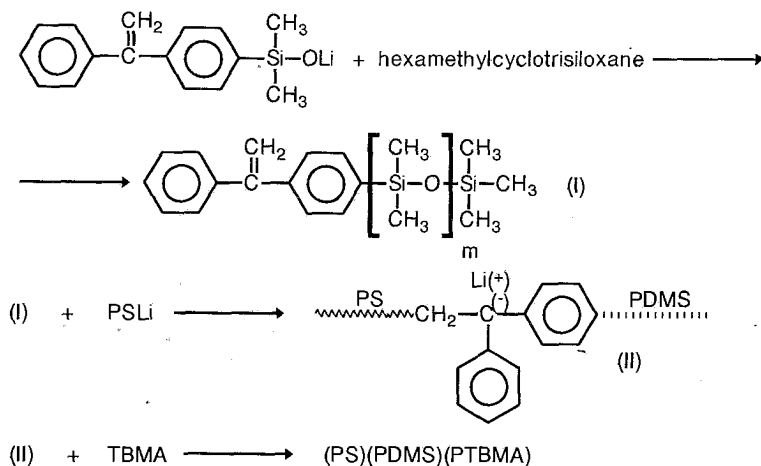
Takano et al. (22) using anionic polymerization techniques and a block copolymer having a multifunctional linking agent at one end, have prepared a miktoarm star copolymer of the A_nB type, where $n=13$, A is polystyrene and B is poly(vinyl - b - naphthalene) (PVN), according to the following:



This method is based on the fact that the vinyl group of the VS monomer is more reactive than the silylvinyl group in a polar solvent. However, one has to be very careful about polymerization time, because the silylvinyl group can react with the living VS anion if it is allowed to stand too long. Anyway, the disadvantage of this approach is that it is difficult to control precisely the number of arms, and a large amount of double bonds remains in the polymer.

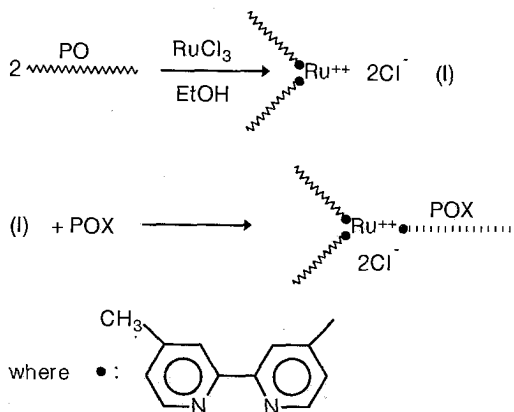
Fujimoto et al. (23) have prepared a 3-miktoarm star terpolymer of the ABC type, where A, B, C are poly(dimethylsiloxane) (PDMS), PS, and poly(t-butylmethacrylate) (PTBMA), respectively. The synthetic approach

involves the coupling of polystyryl anion with a diphenylethylene-capped poly(dimethylsiloxane), followed by anionic propagation of *t*-butylmethacrylate, according to the following reaction scheme:



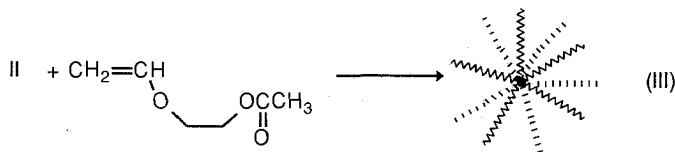
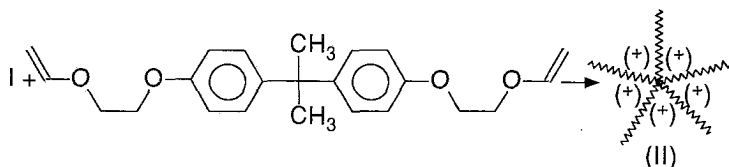
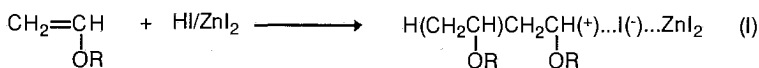
The disadvantages of the method are that fractionation of the capped PDMS is needed, and also it seems that the final 3-arm star has higher polydispersity than the PS precursor.

Naka et al.⁽²⁴⁾, using complexation of bipyridyl-terminated polymers with a Ru(II) ion, were able to prepare 3-miktoarm star polymers of the A₂B type, where A is poly (oxyethylene) (PO) and B polyoxazoline (POX) according to the following reactions:



Unfortunately, no characterization results were given in this communication.

The discovery of living cationic polymerization of vinyl monomers has opened the way to synthesize a variety of polymers with well defined structures⁽²⁵⁾. Kanaoka et al.⁽²⁶⁾, using living cationic polymerization techniques and an appropriate divinyl compound as linking agent, have prepared a miktoarm star copolymer of the A_nB_n type, where $n=10$, A is poly(isobutyl vinyl ether) and B is poly(2-acetoxyethyl vinyl ether). Alkaline hydrolysis of pendant acetoxyethyl groups to hydroxy groups led to an amphiphilic miktoarm star copolymer. The basic reactions used for the synthesis are schematically the following:



This approach is similar to the DVB method and presents similar disadvantages. Unfortunately, only limited characterization results of the miktoarm stars were given in this paper.

PROPERTIES

Dilute-Solutions Properties

In the case of linear diblock copolymers evidence for substantial segregation of the blocks in solution is limited⁽²⁷⁾. This is due to the fact that the two different chains in a diblock are statistically already separated in space and only a limited number of heterocontacts is available for further expansion of the molecule. In the case of A_2B and A_2B_2 ⁽⁹⁾ miktoarm stars, the experimental intrinsic viscosity and hydrodynamic

radii were found to be slightly larger than those theoretically calculated, if no intramolecular segregation is assumed. The same result was also obtained in a selectively θ solvent for one of the two parts. This can be attributed to the increased number of heterocontacts due to the star-shaped architecture of the A_2B and A_2B_2 miktoarm stars.

One characteristic feature of block copolymers is that when they are dispersed in selective solvents (solvent for the one block and non-solvent for the other), the lyophobic blocks will collapse into aggregates, while the lyophilic block will be dissolved and will keep the aggregate in solution. Recently, the influence of chain architecture on the aggregation behavior of PS/PI block copolymers was investigated using SANS, LALLS and viscometry(28).

SANS measurements of the SH block copolymers of the $(PI)_3(PS-d_8)(PI)_3$ type were performed in n-decane. n-Decane is a selectively good solvent for PI and a poor solvent for PS. The measurements were performed at two different contrasts. In each case one of the monomeric units was matched by using as solvent a mixture of protonated and deuterated n-decane. As a consequence the molecular characteristics of the PS-d8 core and the PI corona of the aggregates were obtained. The PS-d8 core is found to be in a melt state since there is no or little solvent in this part of the micelle. On the other hand, the corona consists of swollen and stretched PI chains.

In comparison with the corresponding diblocks with similar total molecular weight and composition, the micelles of the SH copolymers present different molecular characteristics. By distributing the PI part in six equal arms, the solubility is shifted to higher PS compositions, the aggregation number becomes one order of magnitude lower, and the coherent scattering cross sections are modified.

Moreover, in the latter work, the thermodynamic calculation of the total free energy of a spherical micelle was carried out, in the spirit of Liebler. It was shown that the distribution of the PI part into six equal arms increases the coronal free energy, which favors micellar disruption, while the interfacial free energy which favours micellar growth is not strongly influenced. As a consequence, lower aggregation numbers are expected. This result was in very good agreement to the experimental results. Finally, the viscometric results reveal that the micelles behave like hard spheres.

Morphology

Model diblock, triblock and starblock copolymers have been investigated in the past in terms of their bulk morphology at the strong and the weak segregation regimes. These studies revealed that block copolymers microphase-separate forming well defined periodic structures with various symmetries(29,30,31).

The phase behavior of the block copolymers in the bulk, at a given volume fraction, is governed by three factors: The number of statistical segments N , which is proportional to the molecular weight of the polymer chains, the Flory-Huggins interaction parameter χ (a mainly enthalpic term characterizing the repulsions between chain segments), and the architecture of the molecule.

In the case of the A_nB miktoarm block copolymers theoretical work has been done only recently and after the successful synthesis of well defined polymers. Here we summarize the morphological aspects of the A_2B and A_3B miktoarm copolymers as found from their characterization by Transmission Electron Microscopy (TEM)^(32,33).

Bright-field TEM results are shown in Figure 2. For the sample preparation the standard protocols were followed in order to ensure the thermodynamic equilibrium of the polymeric bulk.

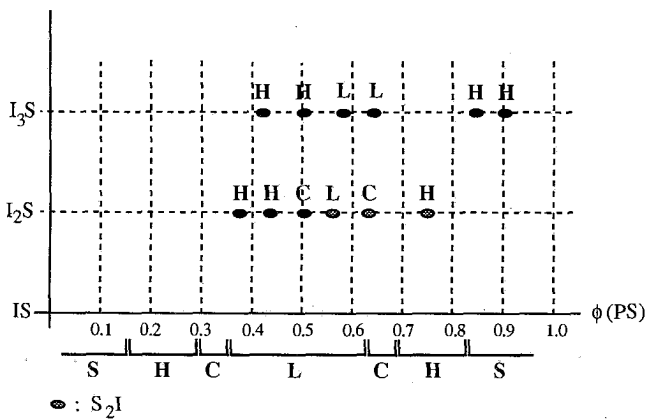


Figure 2
Morphologies of I₂S and I₃S miktoarm stars having various volume fractions of PS

Here L stands for the lamellar morphology, C for the triconnected cubic structures, H for the hexagonally packed cylinders and S for spheres in a body-centered cubic lattice.

Comparing the observed morphologies for the linear diblock copolymers and the miktoarm A_2B and A_3B copolymers it is clear that architecture influences significantly the microdomain structure at a given volume fraction. It is characteristic that in the case of 50% PS the linear diblocks form lamellae, the I₂S miktoarm have a triconnected cubic structure and the I₃S miktoarms form hexagonally packed cylinders of PS in a PI matrix. It is observed that the phase diagram in the SSL (Strong

Segregation Limit) for the diblocks is shifted towards higher volume fractions of PS when PS is the single arm in the miktoarm star. The amount of this shift seems to be larger between the diblocks and the A₂B miktoarms rather than between the A₂B and the A₃B miktoarm copolymers. This can be observed from the volume fraction region where the narrow window of the cubic structures lies. In the case of S2I miktoarm copolymers where the single arm is PIs, the case is reversed and the phase diagram is shifted towards lower PS volume fractions.

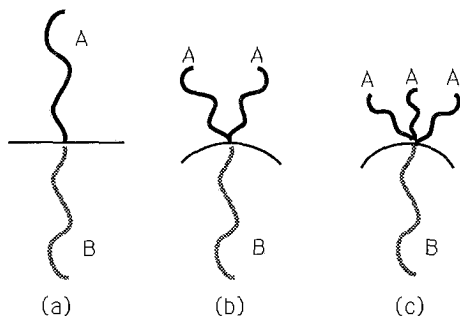


Figure 3

Model for different interfacial curvatures for (a)AB, (b)A₂B and (c)A₃B copolymers with the same composition. The greater crowding on the A side of the interface for the miktoarm case, leads to a greater degree of curvature.

The above mentioned behavior could be explained by taking into account the overcrowding of the chains in one side of the interface, because the same space is now occupied by two or three chains (A₂B and A₃B miktoarms) instead of one (linear diblocks). This will favor a higher degree of curvature of the interface towards the B chain (Figure 3).

An important characteristic observed in the case of I₃S miktoarms is that they do not exhibit the spherical morphology (bcc) at the high PS volume-fraction region. Specifically, the I₃S miktoarm having ca 92% PS by volume, shows order only in a local scale. The micrograph of this polymer shows clearly that it consists of cylinders of PI in a PS matrix. These cylinders assume the hexagonal packing only locally. This observation leads to the conclusion that the sample is very close to the ODT at this volume fraction but still the spherical morphology has not been observed. Due to the high PS content of the polymer it is safe to assume that the spherical morphology is completely eliminated from the phase diagram of these miktoarm copolymers at the high PS content region. The I₃S sample with 85% vol. PS exhibits well ordered hexagonally packed cylinders.

The structure of the I₂S (50% vol. PS) and S₂I (61% vol. PS) miktoarm copolymers was identified as the triconnected cubic. Characteristic TEM projections of these materials exhibited 4-fold symmetry while other projections were 6-fold symmetric. It is well known that only cubic space groups are permitted to have both 4-fold and 3-fold symmetry, in the crystallographic unit cell (the directions (100) and (111) respectively). Also the projection of such a cubic unit cell through the (111) direction belongs to a plane group with a 6-fold axis of symmetry and the same projection through the (100) direction has a 4-fold symmetry axis. In addition the characteristic projections of the materials through the main axes of symmetry were highly similar to the experimentally observed and computer simulated projections of materials that had been identified to be triconnected cubic in the past.

The theoretical approach of Milner⁽³⁴⁾ has been developed in order to predict the structure of these miktoarm copolymer microphases at the SSL. This treatment involves calculations of the chain free energies. In the case of A_nB miktoarms, the A side of the interface contains n times as many chains per unit area as the B so the A arms are much more strongly stretched than the B chains. The total free energy per chain is the sum of the interfacial tension and the increase in stretching free energy. The phase diagram as a function of the volume fraction is then determined by the crossings of the minimized free energies for each structure (lamellar, triconnected cubic, cylindrical and spherical). These minimized free energies are found to depend on the volume fraction and a parameter ϵ , the degree of asymmetry which is defined as: $\epsilon = (n_A/n_B)(l_A/l_B)^{1/2}$ where n_A and n_B are the number of A and B arms and $l = V/R^2$, V and R being the volume and the radius of gyration of each arm in the copolymer. The predicted phase diagram is shown in Figure 4:

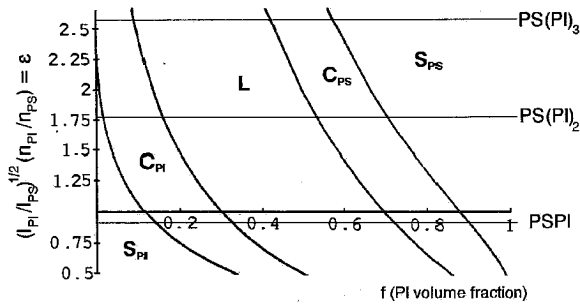


Figure 4

Theoretical phase diagram as a function of the volume fraction

The morphologies observed for the A₂B and A₃B miktoarm copolymers seem to be in a fairly good agreement with those theoretically predicted with the above treatment, at least on a qualitative level. It is seen in the phase diagram that for the A₃B miktoarm copolymers the spherical structure must not be expected in the high PS content region, which confirms the experimental findings. It is also predicted that the triconnected cubic structures should be expected at around 50% vol. PS.

A bulk morphological study⁽³⁵⁾ of the inverse starblock copolymers of PS and PI containing 50% by volume of each component revealed a lamellar to cubic morphology transition when the block asymmetry of these copolymers increases. The block asymmetry is described by the asymmetry parameter α which is defined as the ratio between the outer to the inner block molecular weight. The polymers prepared in this study had $\alpha=1,2$ and 4. When $\alpha=1$ or 2 the lamellar morphology is observed but when α is increased the morphology was changed to cubic. Characterization of the structure by TEM, SAXS and image simulation revealed that the inverse starblock with $\alpha=4$ has a morphology constructed by two interpenetrating PS networks with diamond structure in a PI matrix (OBDD)⁽³⁶⁾. This study proved that:

a. The block copolymer architecture can alter dramatically their morphology even at 50% volume fraction, where the lamellar morphology dominates.

b. The compositionally symmetric inverse starblocks exhibit the OBDD morphology at high degrees of block asymmetry.

c. TEM along with image simulations are sufficient to fully characterize copolymer morphology.

Similar studies⁽³⁷⁾ of the bulk morphology of S-H polymers showed that structure is strongly influenced by the chemical nature of the connector and the volume fraction of the polymer. The interesting new morphologies that these polymers exhibit are not yet fully characterized and reported in the literature.

Rheology

Mc Leish and collaborators⁽³⁸⁾ have prepared two 4-miktoarm star copolymers of PS and PI of the A₂B₂ type by using the chlorosilane approach, and studied the rheological behavior in a range of temperatures from 100°C to 150°C. An interesting feature was the apparent independence of the rheology on temperature in the above temperature range for a sample with 20% by weight PS.

The static and kinetic aspects of the order - disorder transition (ODT) of a 3-miktoarm star terpolymer of SIB type and a 3-miktoarm star copolymer of the SI₂ type, have been studied using SAXS and rheology⁽³⁹⁾. The T_{ODT} was found to be 379K for both polymers. At

temperatures above the T_{ODT} both polymers show a rheological behaviour characteristic of the Newtonian flow of the melt. At temperatures below the T_{ODT} this behavior changes drastically. The time-temperature superposition principle can be successfully applied only at the high frequency parts of G' and G'' frequency dependencies. At low frequencies considerable deviations from the Newtonian flow are observed, as both dependencies of G' and G'' vs. ω become almost parallel and assume the slope 0.33. The ordering kinetics have also been studied. They were analyzed in terms of a nucleation and growth process of the Avrami type. It is interesting that the width of the kinetically accessible metastable region was found to be enlarged as compared to linear diblocks.

Applications

These new materials are expected to find application mainly as compatibilizers of two, three or four different homopolymers. Already the A₂B miktoarm stars are better compatibilizers than the corresponding linear AB(40).

APPENDIX

Anionic Polymerization Techniques

For the successful synthesis of miktoarm star polymers, the sophisticated and rather complicated high vacuum techniques must be used. The aim of these techniques, is the exclusion from the system of undesirable species, as f.e. reactive impurities of the reagents, atmospheric oxygen, moisture or carbon dioxide etc., which can deactivate the initiator or the "living" macroanions.

All manipulations are carried out in high vacuum ($\sim 10^{-6}$ mmHg) using break seals, magnetic breakers guided with an external magnet, and sealoffs for the addition and the removal of the reagents. A typical reactor used for the synthesis of the living linear arm precursors is shown in Figure 5. The purge section is used for purging the apparatus with a solution of n-BuLi in the polymerization solvent, so that any reactive impurity in the glassware is removed. After washing the walls of the apparatus by solvent distillation, the solvent is distilled back into the polymerization flask A and the purge section is sealed off in the constriction (a). Then the monomer and the initiator are added, by breaking the appropriate break seals. Finally, the living polymer is transferred to flask B and the constriction (b) is sealed off. This flask can be joined later, to the main reactor for the linking reaction

The main reactor used for the linking reactions during the synthesis of the miktoarm stars is shown in Figure 6. The purge section is used as described above and it is eventually removed from the reactor. The living arms are added to the reactor through the fingers using the appropriate

break seals as shown in Figure 7. Break seals are also used for the removal of the excess of chlorosilanes, after the attachment of the reactor to the vacuum line. The reactor is also equipped with samplers, used for the removal of small aliquots of the reaction mixture, in order to monitor the reactions, by using the appropriate characterization methods.

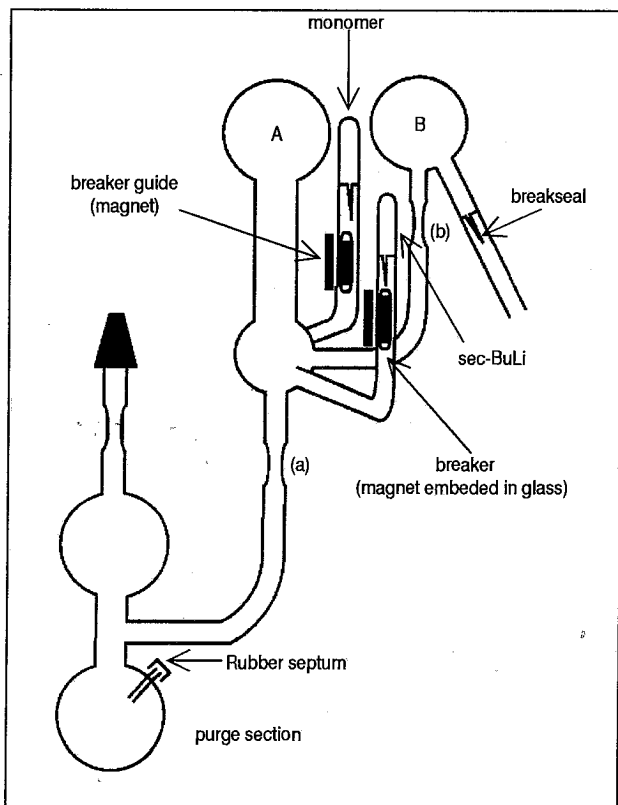


Figure 5
Polymerization apparatus

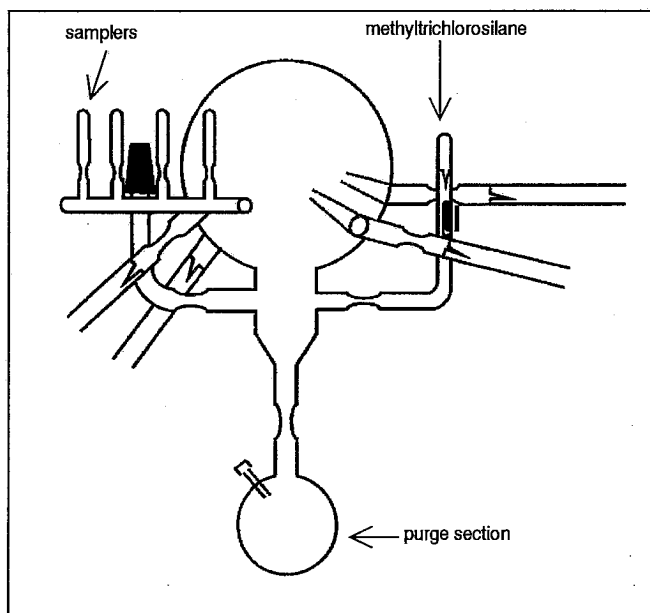


Figure 6
Main reactor for the linking reactions

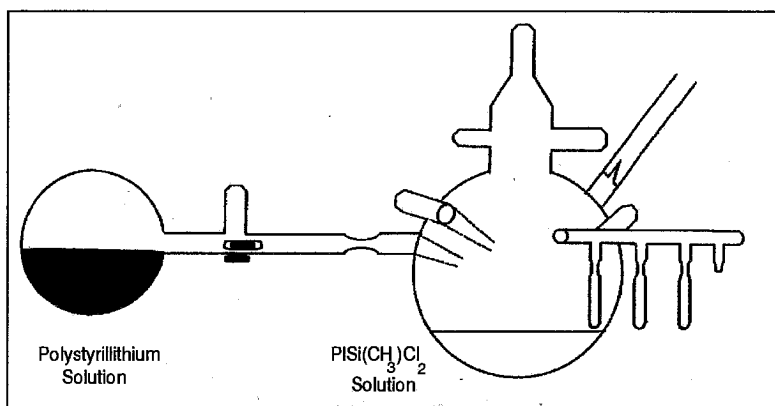


Figure 7
Titrating the macromolecular linking agent

ΠΕΡΙΛΗΨΗ

Σ' αυτό το άρθρο ανασκόπησης, παρουσιάζονται οι μέθοδοι σύνθεσης μικτόχλωνων αστεροειδών πολυμερών, δηλαδή πολυμερών που έχουν χημικά διαφορετικούς κλάδους. Οι περισσότερες μέθοδοι σύνθεσης βασίζονται στον ανιοντικό πολυμερισμό και στη χρήση κατάλληλων μέσων σύζευξης, όπως π.χ. διβυνιλοβενζολίων, διπλών 1,1-διφαινυλαιθυλενίων και χλωροσιλανίων. Επειδή τα πολυμερή αυτά παρασκευάστηκαν πρόσφατα, υπάρχουν μόνο λίγα αποτελέσματα που αφορούν τις ιδιότητές τους σε διαλύματα και σε στερεά κατάσταση. Από τα πρώτα αποτελέσματα φαίνεται ότι τα νέα αυτά υλικά θα ανοίξουν νέους δρόμους στην επιστήμη και τεχνολογία πολυμερών.

Acknowledgments

We would like to express our gratitude to Dr.A.Lovinger (AT&T Bell Laboratories) Associate Editor of "Macromolecules", for revising the manuscript.

REFERENCES

1. H.Eschwey, W. Burchard, *Polymer* **16**,180 (1975)
2. C.Tsitsilianis, P.Chaumont, P.Rempp *Makromol. Chem.* **191**, 2319 (1990)
3. C. Tsitsilianis , S.Graff, P.Rempp *Eur.Polym. J.* **27**,243, (1991)
4. A. Yamagishi, M.Szwarc, L.Tung, Grace Y-S. Lo *Macromolecules*, **11**, 607 (1978)
5. R.P.Quirk, T. Yoo, B. Lee J.M.S.- *Pure Appl. Chem.* **A31**,911 (1994)
6. R.W. Pennisi, L.J.Fetters, *Macromolecules*, **21**, 1094 (1988)
7. M.Morton, T.E.Halminiak, S.D.Gadkary, F.J.Bueche *J.Polym.Sci.* **57**, 471 (1962)
8. J.W.Mays, *Polymer Bull.*, **23**,247 (1990)
9. H.Iatrou, E. Siakali - Kioulafa, N.Hadjichristidis, J.Roovers, J.W. Mays, *J.Polym. Sci.Polym. Phys. Ed.*-accepted
10. Y. Tselikas, N. Hadjichristdis, to be published
11. H.Iatrou, N.Hadjichristidis, *Macromolecules*, **25**, 4649 (1992)
12. H.Iatrou, N.Hadjichristidis, *Macromolecules*, **26**, 2479 (1993)
13. J.Allgaier, R.Young, V.Efstratiadis, N.Hadjichristidis, to be submitted
14. Y. Tselikas, N. Hadjichristdis, to be published
15. R.C.C.Tsiang, *Macromolecules*, **27**, 4399 (1994)
16. H.Iatrou, A.Avgeropoulos, N.Hadjichristidis, *Macromolecules*, **27**, 6232 (1994)
17. J.Roovers, P.Toporowski, *Macromolecules* **14**,1174,1981
18. F.Wang and J.Roovers *Polym. Prepr.* **35**(2), 600, 1994
19. N.Hadjichristidis et all., to be submitted
20. Huynh Ba Gia, R.Jerome, Ph.Tessie, *J. Pol. Sci., Pol.Chem. Ed.*,**18**, 3483 (1980)

21. I.M.Khan, Z.Gao, Khougaj, A. Eisenberg, *Macromolecules*, 25, 3002 (1992)
22. A.Takano, M.Okada, T.Nose, T.Fujimoto, *Macromolecules*, 25, 3596(1992)
23. T.Fujimoto, H.Zhang, T.Kajama, Y.Isono, H.Hasegawa, T.Hashimoto, *Polymer*, 33, 2208, (1992)
24. A.Naka, K.Sada, Y.Chujo, T.Saegusa, *Polym. Prepr. Jpn.*1991, 40(2) E116 (SPSJ Okayama Meeting)
25. M.Sakamoto, *Prog.Polym.Sci.*, 16, 111 (1991)
26. S.Kanaoka, T.Omura, M.Sakamoto, T.Higashimura, *Macromolecules*, 25, 6407 (1992)
27. J.Prud'homme, J.Roovers, S.Bywaters, *Europ. Polym. J.*, 8,901 (1972)
28. H.Iatrou, L.Willner, N.Hadjichristidis, D.Richter, submitted to *Macromolecules*
29. G.E.Molau, *Block Copolymers*, S.L.Agarwal Eds.; Plenum New York, 1970
30. E.L. Thomas, D.M. Anderson, C.S.Henkee, D.Hoffman, *Nature*, 334, 598 (1988)
31. F.S.Bates, G.H.Fredrickson, *Ann.Rev.Phys.Chem.*,41,525 (1990)
32. N.Hadjichristidis et. al. *Macromolecules*, 26, 5812 (1993)
33. Y.Tselikas, H. Iatrou, N.Hadjichristidis, to be submitted
34. S.T.Milner, *Macromolecules* 1994, 27, 2333 (1994)
35. Y.Tselikas, N.Hadjichristidis, E.L.Thomas, submitted
36. E.L.Thomas, D.B.Alward, D.J.Kinning, D.C.Martin, D.L.Handlin, L.J.Fetters, *Macromolecules*, 19, 2197, (1986)
37. N.Hadjichristidis, E.L.Thomas, unpublished results
38. J. Johnson, R.N. Young, S.J. Wright, T. Mc Leish *Polym. Prep.*,35(2), 470 1994
39. G.Floudas, N.Hadjichristidis, H.Iatrou, T.Pakula, E.W.Fischer, *Macromolecules*, 27, 7735 (1994)
40. N. Hadjichristidis, unpublished results

**An ESR Study of Radicals and Radical-cations Generated from the reaction
of some Methoxyphenyl-substituted Alcohols, Aldehydes and Carboxylic
Acids with HO•, SO₄⁻, ^tBuO•, and by Direct Photolysis.**

A. Valavanidis^a, B.C. Gilbert^b and A.C. Whitwood^b

^aDepartment of Chemistry, University of Athens, University Campus, Zografou, 15771,
Athens, Greece.

and

^bDepartment of Chemistry, University of York, Heslington, York. YO1 5DD, England

Received: April 20, 1995

Summary

E.s.r. spectroscopy has been employed to characterize radical-cations and radicals formed by the reaction of some mono-, di-, and tri-methoxyphenyl-substituted alcohols, aldehydes and carboxylic acids with various radical-producing systems: SO₄⁻ was generated photolytically from peroxydisulphate, HO• from Ti^{III}-H₂O₂ in a flow system, and ^tBuO• by *in situ* photolysis of di-*tert*-butyl peroxide. The influence of the methoxy group(s) in the formation and reaction of radical-cations (some of which are detected) has been studied. Reactions characterised include deprotonation and decarboxylation, as well as rapid reduction by Ti^{III}. Other reactions observed include *ipso* attack of HO• and hydrogen abstraction by *t*-butoxyl.

Key words: e.s.r. spectroscopy, free radicals, phenyl-substituted alcohols, aldehydes, carboxylic acids

Introduction

The reactions of phenyl-substituted alcohols, ethers, carboxylic acids and related compounds with various radical-producing systems in aqueous or organic solutions have previously been investigated by e.s.r. spectroscopy. Side-chain oxidations, including loss of a hydrogen atom, and fragmentation by various routes have been observed.¹⁻³ For example, with both HO• (at low pH) and SO₄⁻ in aqueous solution, the side-chain oxidation of phenyl-substituted carboxylic acids proceeds *via* the formation of arene radical-cations which subsequently undergo proton-loss (to give benzylic radicals) or electron transfer from the anionic carboxylate group, followed by decarboxylation.² The reactions of HO• and SO₄⁻ with a number of phenyl-substituted alcohols also provide evidence for fragmentation of first-formed radical-cations, including deprotonation, C_α-C_β bond scission (*eg.* reaction of [PhCH₂CH₂OH]^{•+} to give PhCH₂• and [•]CH₂OH) and longer-range fragmentation.³ Phenyl-substituted ethers react with HO• mainly to give radicals with the loss of a benzylic hydrogen atom *via* the radical-cation; remote oxidation of the side-chain does not occur for the ethers (for which alkylation of oxygen prevents formation of a cyclic intermediate).^{1,4,5} In contrast, ¹BuO• abstracts a hydrogen atom from organic substrates of this type to yield different radicals (usually *via* direct C-H or O-H abstraction), some of which undergo subsequent fragmentation of a different type (*eg.* Ph[•]CHOCH₂Ph → PhCHO + •CH₂Ph).⁶

In this paper, we describe the results of investigations designed to generate a variety of radical-cations and radicals from mono-, di- and tri-methoxyphenyl-substituted alcohols, and the corresponding aldehydes and carboxylic acids and their study by e.s.r. spectroscopy. The radicals were produced by HO• (from reaction of Ti^{III}-H₂O₂ in a flow system), SO₄⁻ (generated photolytically from peroxydisulphate, S₂O₈²⁻) both in aqueous solution, and by reaction with ¹BuO• (generated photolytically from di-*tert*-butyl peroxide); direct photolysis of the substrate was

also studied. We set out in particular to investigate the influence of the electron-donating methoxy substituents on the modes of reaction and on both radical and radical-cation formation, the latter of which would be expected to be greatly facilitated. Some of these compounds have special interest. For example, certain methoxylated substrates, such as veratryl alcohol (3,4-dimethoxybenzyl alcohol), are models for lignin degradation products and their ability to form radicals when oxidized by ligninase (an extra-cellular peroxidase produced by several species of white-rot fungi) has been studied extensively.⁷ It is believed that these and related methoxylated substrates can be oxidized by ligninase to radical-cation intermediates which can undergo C-H or C-C bond cleavage. These radical-cations can also act as oxidants and thus function as mediators, causing oxidation in a polymer not immediately accessible to ligninase. This could be important in the degradation of natural lignocellulose substrates.⁸

The radical-cations of some related species with electron-donating substituents such as methyl, amino or methoxy groups have previously been studied by e.s.r. spectroscopy.^{9,10,11} For example, methoxylated benzoic acid radical-cations have been directly detected in fluid solution with e.s.r. spectroscopy; the presence of even one methoxy group appears to be sufficient to stabilize radical-cations towards decarboxylation.¹²

Experimental

E.s.r. spectra were recorded on a Bruker ESP 300 X-band spectrometer. The hyperfine splittings and g -values were determined from the spectrometer field scan, this having been calibrated with the signal from Fremy's salt (a_N 1.309 mT¹³, g 2.0055¹⁴). All photolyses were carried out using the unfiltered radiation of a Hanovia B-1 1-kW mercury-xenon compact arc.

E.s.r. experiments with HO• involved the use of a three-stream rapid-mixing system by which aqueous solutions were simultaneously mixed a short time (typically *ca.* 30 ms) before

passage through the cavity of the e.s.r. spectrometer and their spectra recorded during continuous-flow. The flow was maintained using a Watson-Marlow 502S flow-inducer positioned on the inlet tubing. The solutions were as follows: stream (i) contained titanium (III) chloride ($2.67 \times 10^{-3} \text{ mol dm}^{-3}$), stream (ii) contained hydrogen peroxide ($1.33 \times 10^{-2} \text{ mol dm}^{-3}$), and the third stream contained the substrate at a concentration of up to 0.05 mol dm^{-3} (all concentrations are those after mixing). Less soluble substrates were divided into three portions and dissolved in each stream. The pH was adjusted by the addition in stream (i) of concentrated sulphuric acid or sodium hydroxide to the first stream. pH measurements were made using a Pye-Unicam PW9410 pH meter with the electrode inserted into the effluent stream. All solutions were deoxygenated both before and during use by purging with oxygen-free nitrogen.

Experiments with $\text{SO}_4^{\cdot-}$ involved the use of *in situ* photolysis and were carried out in a typical flat aqueous cell with a built-in two-way mixer through which the solutions were forced by gravity (flow-rate 2 ml min^{-1}). The two streams (deoxygenated as above) typically contained $\text{Na}_2\text{S}_2\text{O}_8$ (either 0.1 or 0.05 mol dm^{-3}) and the substrate (0.005 - 0.1 mol dm^{-3} , with 0.3 mol dm^{-3} acetone).

Experiments with the *t*-butoxyl radical were carried out by *in situ* photolysis of static samples using solutions of di-*tert*-butyl peroxide (5% v/v) and the substrate (10% v/v) in benzene. The temperature was typically maintained at 273 K using the Bruker ER-4111 attachment. Prior to photolysis, solutions were deoxygenated by purging with oxygen-free nitrogen for 5 minutes. Experiments were also conducted under direct photolysis using solutions of the substrates (10% v/v) in benzene.

Spectral simulations were carried out using a program (kindly provided by Dr. M.F. Chiu) in which exchange and second-order effects were incorporated. The program was modified to run on a VAX mainframe computer, an IBM 486DX clone and on a BBC microcomputer.

Chemicals and solvents were commercially available and used without further purification.

Results and Discussion

a) Reactions of some Methoxyphenyl-substituted Alcohols

Initial experiments involved the reaction of HO• with the methoxyphenyl-substituted alcohols shown in Table 1. For 4-methoxybenzyl alcohol and 2-(4-methoxyphenyl)ethanol reaction in the pH range 3.0-9.5 gave complex e.s.r. spectra assigned to a mixture of hydroxycyclohexadienyl adducts for which individual assignments were not possible; however, as the pH was lowered below 2, signals from the appropriate phenoxy radicals were obtained. 3,4-Dimethoxybenzyl alcohol and 3,4,5-trimethoxybenzyl alcohol behaved in a similar fashion and at low pH gave a spectrum dominated by a single phenoxy radical (with the phenoxy oxygen *para* to the substituent) as shown in Table 1.

We conclude that the phenoxy radical is formed by an acid-catalysed process and propose a reaction involving loss of methanol from the appropriate *ipso* adduct (see Scheme 1). The effective route to the *ipso* adduct may involve either HO• attack at the *ipso* position in the parent compound or hydration of a radical-cation formed by loss of water after protonation of the cyclohexadienyl adduct (or both). Two previous findings (that anisole-type radical-cations are not rapidly hydrolysed¹⁰ and that they are readily susceptible to reduction by low valent transition-metal ions²) strongly suggest that the latter pathway is not the source of the phenoxy radicals; we might have expected, on the basis of previous work,⁴ that reaction would be accompanied by loss of an α -proton or $-\text{CH}_2\text{OH}$, neither of which pathway was observed (but see below). This suggests that *direct* attack of HO• at the *ipso* position, with acid-catalysed loss of methanol, is responsible for the observed behaviour (see Scheme 1), and that radical-cations, if formed, are readily reduced by titanium (III). To test this hypothesis, we attempted to generate the radical-

cations independently by reaction of the parent alcohols with $\text{SO}_4^{\cdot-}$.

In accord with expectation, reaction of $\text{SO}_4^{\cdot-}$ with 3,4-dimethoxybenzyl alcohol and 3,4,5-trimethoxybenzyl alcohol gave spectra which are assigned to the appropriate radical-cation (on the basis of splittings for related species reported in references 10 and 11, see Table 1 and Figure 1, 3,4-dimethoxybenzene radical-cation itself has large hyperfine splittings from the protons *para* to the methoxy groups). There was no evidence for hydrolysis of the radical-cation or deprotonation from the benzylic position under the conditions employed. Under similar conditions, 4-methoxybenzyl alcohol gave a single broad line, evidently due to the formation of an insoluble material on the surface of the ESR cell.

In the reaction of the substrates with $^t\text{BuO}^\bullet$, hydrogen-abstraction was observed to give the hydroxy-conjugated radicals (see Table 1 and, for example, Figure 2) as expected for reaction of an electrophilic radical which favours hydrogen-abstraction rather than addition.

b) Reactions of some Methoxy-substituted Benzaldehyde derivatives

Reaction of HO^\bullet with a variety of methoxylated benzaldehydes at higher pH (>3) also gave a mixture of cyclohexadienyl adducts. On lowering the pH, new signals were seen from both the appropriate phenoxy radicals and also the appropriate acyl radicals (clearly characterised by their low *g*-value and narrow overall splitting pattern, for examples, see Table 2). This behaviour was observed below pH 2 for the 3,4-dimethoxybenzaldehyde and 3,4,5-trimethoxybenzaldehyde, and at a somewhat lower pH for 4-methoxybenzaldehyde. We believe that the phenoxy radicals observed are again derived from to *ipso* attack of HO^\bullet (analogous to the reaction of HO^\bullet with the alcohols at low pH, cf. Scheme 1) and that the benzoyl (acyl) radicals derive from abstraction of the aldehydic proton. The presence of the acyl group evidently retards the formation of the radical-cation (as observed by the lower pH required for dehydration of the initial HO^\bullet adduct).

The lack of direct observation of the radical-cation is again believed to be due to reduction by the Ti^{III} . Consistent with this is the observation that reaction of $SO_4^{\cdot-}$ with 3,4-dimethoxybenzaldehyde and 3,4,5-trimethoxybenzaldehyde gave signals assigned to the corresponding radical-cations (see Table 2). The splittings of the radical-cation of 3,4,5-trimethoxybenzaldehyde could not be determined accurately; this is believed to be due to the presence of other signals possibly arising from direct photolysis. 4-Methoxybenzaldehyde gave a single broad line due to photolysis of insoluble products which had precipitated onto the ESR cell wall.

The number and magnitude of the hyperfine splittings and g -values of the radical-cations from 3,4-dimethoxybenzaldehyde and 3,4,5-trimethoxybenzaldehyde are very similar to those of the non-aldehydic analogues^{10,11} so the extra large splitting observed, compared with expectation, must be due to the aldehyde proton. By implication, the spin-distributions in the benzaldehyde radical-cations will also resemble those of the parents. Hence, in these two radical-cations there must be very little spin-density on the carbonyl carbon. The large aldehyde proton splitting must arise from interaction of this proton with the orbital on the *ipso* carbon (*i.e.* it is a β -splitting, not an α -splitting). In order to give rise to such a large splitting, the aldehyde group must be rotated out of the plane of the aromatic ring and therefore not conjugated with it. This phenomenon will be investigated further with a range of di- and tri-methoxylated benzaldehydes and results presented in a later paper.

Direct photolysis of the substrates in benzene was found to give rise largely to the appropriate acyl radical. It is believed that irradiation gives the relevant radical-cation (*via* intramolecular electron-transfer) which decomposes by loss of the formyl proton under these conditions. Reaction of benzaldehydes with $^tBuO^{\cdot}$ also gives acyl radicals. This probably occurs by hydrogen abstraction by $^tBuO^{\cdot}$ although a contribution from formation of the radical-cation

by direct photolysis cannot be ruled out.

c) Reactions of Methoxy-substituted Phenylacetic Acids

Reaction of $\text{HO}\cdot$ with (4-methoxyphenyl)acetic acid at low pH (pH less than 2) led to the formation of the 4-methoxybenzyl radical evidently due to rapid decarboxylation of the radical-cation. With (3,4-dimethoxyphenyl)acetic and (3,4,5-trimethoxyphenyl)acetic acids the appropriate phenoxyl radicals are observed, evidently arising from *ipso* attack of $\text{HO}\cdot$. We believe that for the monomethoxylated compound, the radical-cation is formed, but not now readily reduced (the effect of the single +M methoxy group is offset to some extent by the -I effect of the acid group) and therefore fragmentation (decarboxylation) ensues (see Scheme 2 and *cf.* reference 2). For the di- and tri-methoxylated acids, radical-cation formation and reduction is rapid with the electronic effects of more than one methoxy group outweighing the influence of the $\text{CH}_2\text{CO}_2\text{H}$ group (*cf.* Scheme 1).

The appropriate methoxylated benzyl radicals were observed in the reaction of the mono-, di- and tri-methoxy-substituted phenylacetic acids with $\text{SO}_4^{\cdot-}$. These observations can be understood in terms of formation of the appropriate radical-cation, as expected, followed by rapid decarboxylation (in the absence of the reducing metal ion); the carboxylate groups would be expected to be ionised under the reaction conditions thus facilitating fragmentation.

Direct photolysis in benzene gave the appropriate benzyl radical; this is again believed to involve production of the radical-cations which then undergo rapid deprotonation and decarboxylation.

The *t*-butoxyl radical reacts *via* hydrogen-abstraction to give the carboxyl-conjugated benzylic species (this would be expected to be the most stable radical due to conjugation of the unpaired electron with both the aromatic ring and the carboxyl group). For the

(3,4-dimethoxyphenyl)acetic acid [and, to a lesser extent, the (3,4,5-trimethoxyphenyl)acetic acid] direct photolysis also occurs to give the radical-cation and hence the benzyl radical formed by decarboxylation (see Figure 3).

d) Formation of Phenoxy Radicals

Addition of HO• to the substrates under acidic conditions would be expected to give at least a proportion of the *ipso* adduct (other adducts probably give radical-cations *via* loss of water). This can then undergo acid-catalysed loss of methanol to give the phenoxy radical.

Where two or more phenoxy radicals could, in principle, be formed (*i.e.* with the di- and tri-methoxylated substrates), only the *para*-substituted species is clearly observed. At least three reasons for this apparent selectivity can be suggested; the cyclohexadienyl precursor of the *para*-substituted phenoxy is likely to be the most stable of the possible hydroxyl adducts, the *para*-substituted phenoxy radical (most hindered) would be expected to have the slowest rate of radical-radical termination and, finally, the higher symmetry of the *para*-substituted species will make the signals apparently more intense at any given radical concentration compared to that of the less symmetrical species. Further studies are unjustified.

Conclusions

The results obtained from •OH with all substituents are consistent with predominance of initial attack on the aromatic to give hydroxyl adducts at higher pH; For the methoxylated benzaldehydes, direct abstraction of the acyl hydrogen also occurs (a reaction which predominates for *t*-butoxyl). At lower pH (below pH 2.0) acid-catalysed dehydration of the cyclohexadienyl adducts occurs to give the appropriate radical-cation, which subsequently undergoes fragmentation (*e.g.* decarboxylation) or reduction by titanium(III). The role of the methoxy

groups (which have a relatively strong electron-donating ability) in the reduction of the charge-density of the ring, by localising charge onto oxygen, is very important in governing the ease of radical-cation formation and subsequent reactions. For HO• adducts, *ipso* to a methoxy group, acid-catalysed loss of methanol (and subsequently the hydroxyl proton) leads to the formation of phenoxyl radicals.

The radical-cations derived from the 3,4-di- and 3,4,5-tri-methoxylated benzyl alcohols and benzaldehydes have been generated and characterised by ESR in the reaction of the parent compound with $\text{SO}_4^{\cdot-}$ (generated photolytically from $\text{S}_2\text{O}_8^{2-}$). Hyperfine splittings for these radical-cations were found to closely resemble the radical-cations of 1,2-dimethoxybenzene and 1,2,3-trimethoxybenzene, respectively.^{10,11} Large splittings arising from the aldehyde protons are believed to be symptomatic of the aldehyde groups being rotated out of conjugation with the aromatic ring in these species.

The radical-cations derived from the methoxylated phenylacetic acids (with $\text{SO}_4^{\cdot-}$) undergo rapid electron-transfer from the carboxylate group onto the aromatic ring, with subsequent decarboxylation to give the appropriate benzyl radicals.

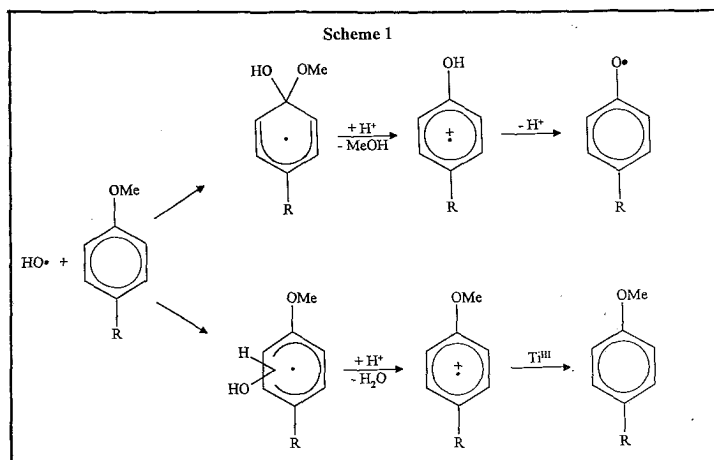
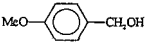
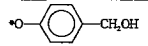
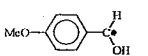
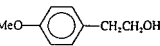
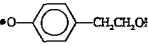
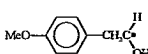
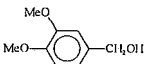
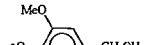
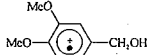
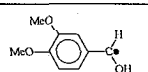
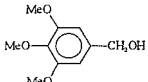
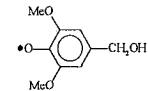
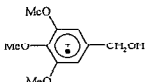
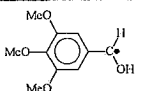


Table 1
E.S.R. Parameters of Radicals Generated from Reactions of Methoxyphenyl-substituted Alcohols with HO^\bullet , $\text{SO}_4^{\bullet-}$, t-BuO^\bullet and Direct Photolysis (Methods A, B, C and D, respectively)

Substrate	Method	Radical detected	Hyperfine Splittings (mT) ^b					g-value
			a(α -H)	a(β -H)	a(2,6-H)	a(3,5-H)	a(others)	
 4-Methoxybenzyl alcohol	A		-	-	0.61	0.15	0.86 (CH ₂)	2.0043
	C,D		1.525	-	0.53 (1H) 0.43 (1H)	0.15	0.05 (4-OMe)	2.0032
 2-(4-Methoxyphenyl)ethanol	A		-	-	0.61	0.15	0.75 (CH ₂)	2.0043
	C		1.50	2.13	-	-	-	2.0033
 3,4-Dimethoxybenzyl alcohol	A		-	-	0.61	0.15	0.86 (CH ₂)	2.0043
	B		-	-	0.49 (1H) ^d	-	1.065 (CH ₂) 0.34 (OMe) 0.30 (OMe) 0.06 (OH)	2.0032
	C,D		1.49	-	0.53 (1H) 0.43 (1H)	0.16	0.05 (4-OMe)	2.0034
 3,4,5-Trimethoxybenzyl alcohol	A		-	-	-	0.13	0.86 (CH ₂) 0.13 (2,6-OMe)	2.0045
	B		-	-	0.02	-	1.10 (CH ₂) 0.495 (4-OMe) 0.19 (3,5-OMe)	2.0034
	C,D		1.48	-	0.48	-	-	2.0031


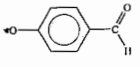
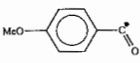
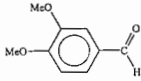
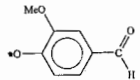
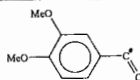
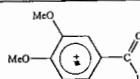
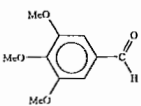
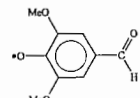
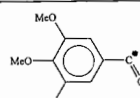
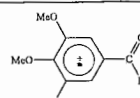
^bHydroxycyclohexadienyl radicals were detected from each substrate at higher pH. Data refer to acidic conditions (pH < 2)

^b ± 0.01 mT

^c ± 0.0001

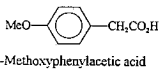
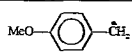
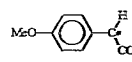
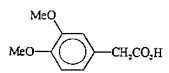
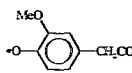
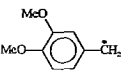
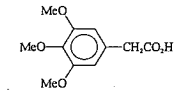
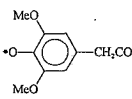
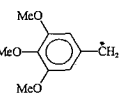
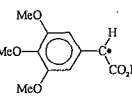
^d From the 6-proton

Table 2
E.S.R. Parameters of Radicals Generated from Reactions of Methoxy-substituted Benzaldehydes with HO^\bullet , $\text{SO}_4^{\bullet-}$, $^t\text{BuO}^\bullet$ and Direct Photolysis (Methods A, B, C and D, respectively)

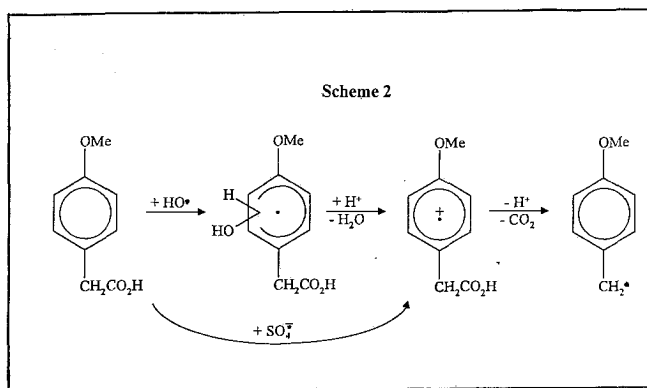
Substrate	Method	Radical detected	Hyperfine Splittings (mT) ^b				
			a(α -H)	a(2,6-H)	a(3,5-H)	a(other)	g-value ^c
 4-Methoxybenzaldehyde	A, C ^d		-	0.61	0.14	-	2.0043
	A, C, D		-	0.10	0.15	-	2.0004
 3,4-Dimethoxybenzaldehyde	A, C ^d		-	0.62	0.14	0.14 (2-OMe)	2.0043
	A, C		-	0.10	-	-	2.0004
	B		-	0.480 (1H) ^e	0.035 (1H)	0.335 (3-OMe) 0.335 (4-OMe) 0.510 (CH=O)	2.0034
 3,4,5-Trimethoxybenzaldehyde	A, C ^d		-	-	0.14	0.14 (2,6-OMe)	2.0043
	A, C		-	0.01	-	-	2.0004
	B ^f		-	0.035	-	0.515 (4-OMe) 0.190 (3-OMe) 0.190 (5-OMe) 0.650 (CH=O)	2.0035

^bHydroxycyclohexadienyl radicals were detected from each substrate at higher pH. Data refer to acidic conditions (pH < 2).
^c ± 0.01 mT ^d ± 0.0001 ^eTrace of phenoxyl radical only ^fFrom the 6-proton ^gTentative assignment, splittings ± 0.02 mT

Table 3
E.S.R. Parameters of Radicals Generated from Reactions of Methoxy-substituted Phenylacetic acids with HO•, SO₄^{•-}, tBuO• and Direct Photolysis (Methods A, B, C and D, respectively)

Substrate	Method	Radical detected	Hyperfine Splittings (mT) ^b				
			a(α-H)	a(2,6-H)	a(3,5-H)	a(other)	g-value ^c
 4-Methoxyphenylacetic acid	A, B, D		1.56	0.51	0.16	0.07 (4-OMe)	2.0033
	C		1.35	0.43	0.09	0.09 (4-OMe)	2.0036
 3,4-Dimethoxyphenylacetic acid	A		-	0.61	0.13 (1H) 0.15 (1H)	0.13 (2-OMe) 0.71 (CH ₂)	2.0043
	B, C, D		1.57	0.415 0.60	0.17	0.07 (4-OMe)	2.0031
Substrate	Method	Radical detected	Hyperfine Splittings (mT) ^b				
 3,4,5-Trimethoxyphenylacetic acid	A		-	-	0.13	0.13 (2,6-OMe) 0.80 (CH ₂)	2.0043
	B, C, D		1.54	0.50	-	-	2.0029
	C		1.54	0.48	-	-	2.0036

^aHydroxycyclohexadienyl radicals were detected from each substrate at higher pH. Data refer to acidic conditions (pH < 2).
^b± 0.01 mT ^c± 0.0001



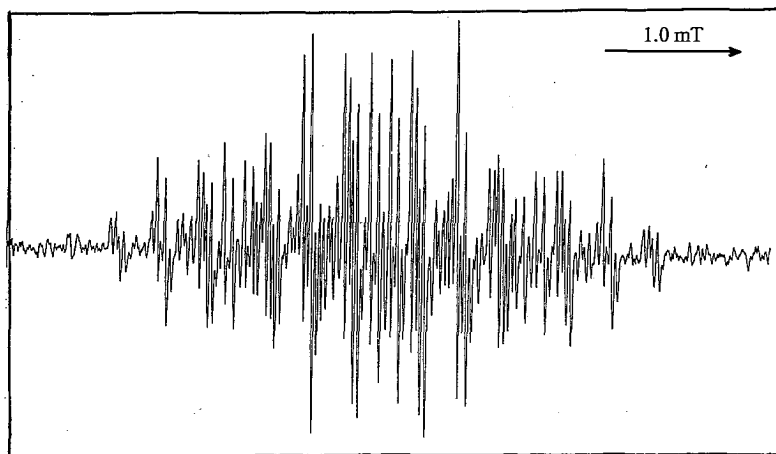


Figure 1. ESR spectrum of the 3,4-dimethoxybenzyl alcohol radical-cation obtained by *in situ* photolysis of an aqueous solution containing $\text{Na}_2\text{S}_2\text{O}_8$ (0.1 mol dm^{-3}), acetone (0.3 mol dm^{-3}) and 3,4-dimethoxybenzyl alcohol ($2 \times 10^{-3} \text{ mol dm}^{-3}$).

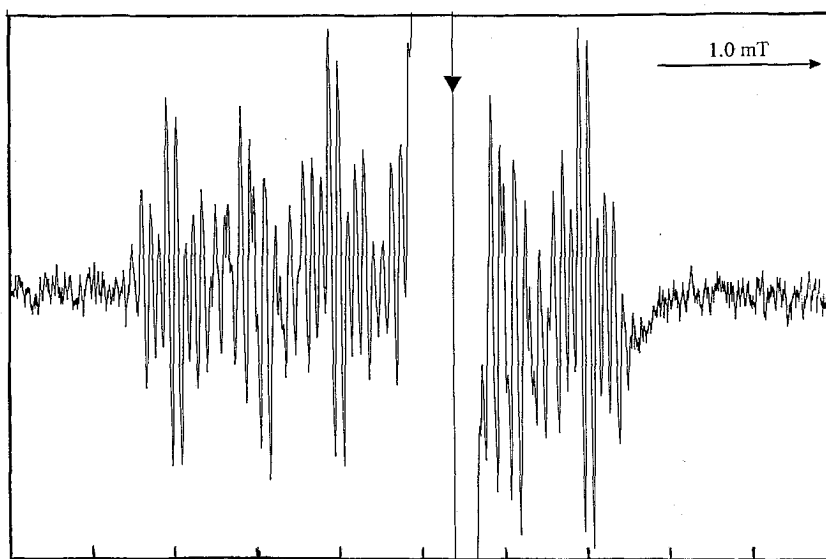


Figure 2. ESR spectrum of the α -hydroxy-4-methoxybenzyl radical obtained by *in situ* photolysis of a benzene solution containing 4-methoxybenzyl alcohol (10% v/v) and di-*t*-butyl peroxide (5% v/v). The signal marked ▼ is due to a radical present in the quartz cell.

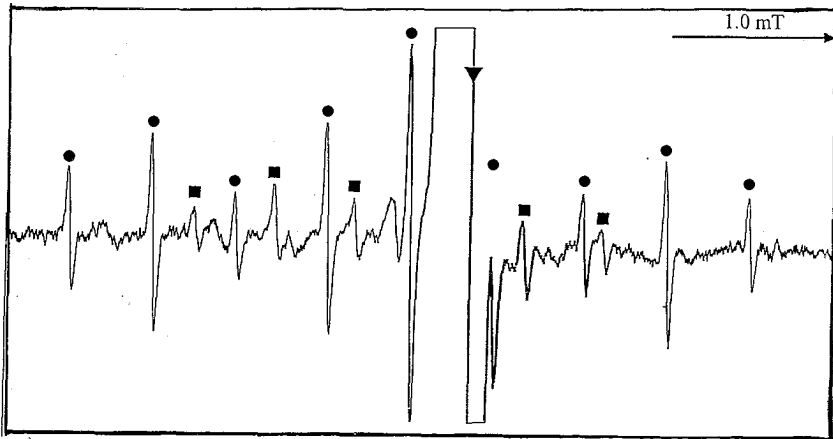


Figure 3. ESR spectrum of the 3,4,5-trimethoxybenzyl radical (●) and the α -carboxyl-3,4,5-trimethoxybenzyl radical (■) obtained by *in situ* photolysis of a benzene solution containing 3,4,5-trimethoxyphenylacetic acid (10% v/v) and di-*t*-butyl peroxide (5% v/v). The signal marked ▼ is due to a radical present in the quartz cell.

Περίληψη

Η φασματοσκοπία Ηλεκτρονικού Παραμαγνητικού Συντονισμού χρησιμοποιήθηκε για τον χαρακτηρισμό των ελεύθερων ριζών που σχηματίσθηκαν από μονο-, δι-, και τρι-μεθοξυφαινυλο-υποκατεστημένες αλκοόλες, αλδεύδες και υποκατεστημένα καρβοξυλικά οξέα. Οι ελεύθερες ρίζες δημιουργήθηκαν με την επίδραση συστημάτων : $\text{SO}_4^{\cdot-}$ από φωτολυτικά διάσπαση του υπεροξυσουλφονικού νατρίου, ρίζες υδροξυλίου (HO^\bullet) με σύστημα συνεχούς ροής των αντιδραστηρίων $\text{Ti}^{\text{III}}-\text{H}_2\text{O}_2$, και $^t\text{BuO}^\bullet$ με την ψτόλυση στην κυψελίδα (*in situ*) του δις-*tert*-βουτυλο υπεροξειδίου. Μελετήθηκε η επίδραση των μέθοξυ- ομάδων στον σχηματισμό και τις αντιδράσεις των κατιόντων-ριζών (μερικές από τις οποίες ανιχνεύθηκαν). Οι αντιδράσεις που χαρακτηρίσθηκαν κατά τις πειραματικές διεργασίες περιελάμβαναν αποπρωτονίωση και αποκαρβοξυλίωση, καθώς και ταχύτατη αναγωγή από το Ti^{III} . Άλλες αντιδράσεις που παρατηρήθηκαν ήταν η *ipso* προσβολή από HO^\bullet και η αφαίρεση υδρογόνου με την επίδραση $^t\text{BuO}^\bullet$.

Λέξεις κλειδιά : ηλεκτρονικός παραμαγνητικός συντονισμός, ελεύθερες ρίζες, φαινυλο- υποκατεστημένες αλκοόλες, αλδεύδες, καρβοξυλικά οξέα

References

1. M.J. Davies, B.C. Gilbert, C.W. McClelland, C.B. Thomas and J. Young, *J. Chem. Soc. Chem. Comm.*, 1984, 966.
2. B.C. Gilbert, C.J. Scarratt, C.B. Thomas and J. Young, *J. Chem. Soc. Perkin Trans. 2*, 1987, 371.
3. B.C. Gilbert and C.J. Warren, *Res. Chem. Intermediates*, 1989, **11**, 1.
4. B.C. Gilbert and C.W. McClelland, "Cyclization of γ -Arylkalknols via Aryl Radical-Cation and Alkoxy Radical Intermediates". 5th International Symposium on Organic Free Radicals. In: H. Fischer and H. Heingartner (eds). *Organic Free Radicals*. Springer-Verlag, Berlin, 1988, p121.
5. B.C. Gilbert, A. Valavanidis and A.C. Whitwood, *Chimika Chronika, New Series*, 1993, **22**, 65.
6. S. Steenken, H.-P. Schuchmann and C. von Sonntag, *J. Phys. Chem.*, 1975, **79**, 763.
7. H.W.H. Schidt, D. Haemmerli, H.E. Schoemaker and M.S.A. Leisola, *Biochem.*, 1989, **28**, 1776.
8. J.M. Palmer, P.J. Harvey and H.E. Schoemaker, *Phil. Trans. R. Soc. London*, 1987, **A321**, 495.
9. P. O'Neill, S. Steenken and D. Schulte-Frohlinde, *Angew. Chem., Int. Ed. Engl.*, 1975, **14**, 430.
10. P. O'Neill, S. Steenken and D. Schulte-Frohlinde, *J. Phys. Chem.*, 1975, **79**, 2773.
11. W.T. Dixon and D. Murphy, *J. Chem. Soc. Perkin Trans. 2*, 1976, 1823.
12. S. Steenken, P. O'Neill and D. Schulte-Frohlinde, *J. Phys. Chem.*, 1977, **81**, 26.
13. R.J. Faber and G.K. Fraenkel, *J. Chem. Phys.*, 1967, **47**, 2462.
14. J.Q. Adams, S.W. Nicksic and J.R. Thomas, *J. Chem. Phys.*, 1966, **45**, 654.

Chimika Chronika, New Series, 24, 233-252 (1995)

METAL-LIGAND π BONDING IN $LM(CO)_5$ COMPLEXES - A VIBRATIONAL SPECTROSCOPY STUDY

M.S. DAVIES, R.S. ARMSTRONG, M.J. ARONEY

Department of Inorganic Chemistry, University of Sydney, Sydney, N.S.W. 2006, Australia

(Received August 3, 1995)

SUMMARY

A systematic study is reported of infrared and Raman band positions and relative band intensities of particular vibration modes for a series of $LM(CO)_5$ complexes (L is amine, phosphine or a related ligand; M is a chromium triad metal). Trends in the data are analysed to ascertain, more definitively than before, the relative π -bonding abilities of the ligands L. From Raman band intensities, a high order of polarisability is found for bonds between M and PBr_3 , providing strong evidence for substantial π character. The results suggest little involvement of E-Y σ^* antibonding orbitals in the receptor mechanism for π -backbonding to coordinated EY_3 .

Key words: infrared, Raman, vibrational spectra, intensity, π -backbonding

INTRODUCTION

Vibrational spectra of complexes $LM(CO)_5$, where L is amine, phosphine or a related ligand and M is a chromium triad metal, have been much studied over some thirty five years. This interest stems primarily from the characteristic high intensity of carbonyl absorptions in the infrared, the relative isolation of these in regard to other bands and from the acute sensitivity of carbonyl positions to the electronic nature of the ligand L.

The present work is part of a multi-technique investigation into possible metal-ligand (M-L) π bonding in these systems.¹⁻⁶ A systematic study of the infrared and Raman band positions of the $\nu(CO)$, $\nu(MC)$ and $\nu(ML)$ vibrations and of relative band intensities is reported for an extensive series of complexes where the ligands L encompass a broad range of steric and electronic properties.

EXPERIMENTAL

Synthesis and purification of the $LM(CO)_5$ complexes as well as details of handling procedures have been described before.¹⁻⁶

Infrared spectra were recorded using a DIGILAB FTS-80 Fourier transform infrared spectrometer equipped with two optical benches, FTS 15/80 and 20/80 configured for far- and mid-infrared regions respectively. Far-infrared spectra were obtained using a 1.0 mm separation solution cell with polythene windows; for mid-infrared spectra a cell with KBr windows of 0.1 mm separation was used.

Raman spectra were determined using a Spectra-Physics Model 2025-11 Kr⁺ or 2025-05 Ar⁺ laser. The wavelengths chosen are sufficiently distant from the electronic absorption bands to preclude any preresonance effects. Solution samples were held in a quartz cell spinning at 1600 rev min⁻¹. Radiation scattered at 90° to the incident was focussed onto the slits of a Jobin-Yvon U1000 double monochromator equipped with a cooled RCA C31034 photomultiplier and photon counting electronics. Scanning and spectral acquisition were computer controlled using a Hicom AT personal computer with ISA Enhanced Prism Software (versions 2.1 and 3.0) The spectra were plotted using a Hewlett-Packard 7475 graphics plotter.

The intensities were calculated by measuring the peak areas, using the in-house JPLOT spectroscopic software package, relative to a standard solvent peak. The peak areas were divided by the molar concentration of the compound and then by the area of the solvent peak to give a normalised area which could be compared directly with results from other spectra.

The complexes were examined in cyclopentane solution since it is a non-interacting solvent with absence of bands in proximity to those of the $\text{LM}(\text{CO})_5$ complexes. Because of low solubility of the $\text{P}(\text{OCH}_2)_3\text{CCH}_3\text{M}(\text{CO})_5$ complexes in cyclopentane, the spectral measurements were made in tetrahydrofuran. Raman spectra for these complexes were also obtained in benzene; no significant band position variations were observed between the spectra in the two solvents.

RESULTS AND DISCUSSION

The $\text{LM}(\text{CO})_5$ complexes examined in this study have C_{4v} local symmetry about the metal atom. Of prime interest are the totally symmetric A_1 stretching modes of the metal-carbon, metal-ligand, and carbon-oxygen bonds as these are polarised along the molecular $\text{L-M-CO}(\text{trans})$ axis. In C_{4v} symmetry, the metal-carbon and carbon-oxygen stretching vibrations have 3 and 4 active components in the infrared and Raman spectra, respectively (see representations on p. 1315 of ref. 7).

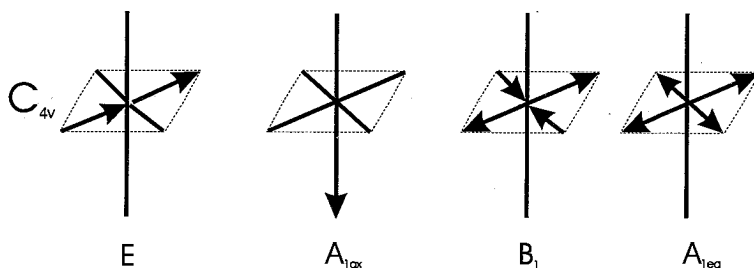


Fig. 1 Stretching Modes of the Metal-Carbon and Carbon-Oxygen
Vibrations in $\text{LM}(\text{CO})_5$ (C_{4v}) Complexes.*

For the CO and MC stretching vibrations, the A_{1eq} , A_{1ax} and E modes are infrared active and the A_{1eq} , A_{1ax} , B_1 and E modes are Raman active. The metal-ligand (M-L) stretching vibration has A_1 symmetry which is both infrared and Raman allowed. Other vibrations have been identified including $\delta(\text{MCO})$, $\delta(\text{CMC})$ and $\delta(\text{LMC})$, but are not further discussed.

Lowering the C_{4v} symmetry for the $\text{LM}(\text{CO})_5$ complexes can arise because of the symmetry, steric bulk and electronic properties of L and this is often reflected in the activation of the infrared forbidden B_1 band in the carbonyl stretching region.⁸⁻¹⁴ Other effects, such as the splitting of the doubly-degenerate E mode, are usually not observed.

Infrared and Raman carbonyl band assignments are given in Table 1; those for the metal-carbon bands are in Table 2; metal-ligand (ML) band positions and relative Raman intensities are listed in Table 3; band positions of $\nu(\text{EY})$ and of $\delta(\text{Y E Y})$ deformations for EY_3 molecules in the free and in the complexed states are shown in Table 4.[†] Metal-carbonyl deformation bands and infrared carbonyl and M-C band intensities are not shown in this paper. These data and the spectra of a range of $\text{LM}(\text{CO})_5$ complexes are to be found in pp. 194-238 of ref. 15.

Infrared and Raman spectra of the $\text{LM}(\text{CO})_5$ complexes in the carbonyl stretching region

Assignments of the carbonyl infrared absorptions are based upon the relative intensities of the bands. From Orgel,¹⁶ the E mode, being non-totally symmetric, is more intense than the two A_1 modes. As the B_1 mode is infrared forbidden, if observed at all, it is very weak. Polarised Raman spectra were carried out confirming the assignments. Unlike the infrared absorptions, the Raman intensities for the $\nu(\text{CO})\text{E}$ mode are found to be very weak.¹⁷ The polarisation properties of the two $\nu(\text{CO})A_1$ modes differ substantially as has been reported previously.¹⁷⁻¹⁹

* From ref. 7; only one component of the degenerate E mode is shown.

[†] It should be noted that wavenumbers are not a measure of frequency which should strictly be measured in Hz. However, common usage has resulted in frequencies being reported in cm^{-1} and this is followed in the present work.

Table 1 Infrared and Raman Carbonyl Band Positions of LM(CO)₅ Complexes in Cyclopentane (cm⁻¹).^a

Complex	$\nu(\text{CO})A_{1eq}$		$\nu(\text{CO})B_1$		$\nu(\text{CO})A_{1ax}$		$\nu(\text{CO})E$	
	IR	R	IR	R	IR	R	IR	R
PCl ₃ Cr(CO) ₅	2088	2087	-	2016	2000	2000	1983	1983
PCl ₃ W(CO) ₅	2094	2094	-	2011	1994	1994	1980	1977
PBr ₃ Cr(CO) ₅	2085	2083	-	2015	1998	1996	1983	1981
PBr ₃ W(CO) ₅	2092	2091	-	2011	1991	1990	1981	1979
P(OCH ₂) ₃ CCH ₃ Cr(CO) ₅ ^b	2077	2077	1994	1994	1955	1958	1955	1955
P(OCH ₂) ₃ CCH ₃ Mo(CO) ₅ ^b	2083	2082	1998	1997	1959	1960	1959	1960
P(OCH ₂) ₃ CCH ₃ W(CO) ₅ ^b	2083	2082	1989	1990	1952	1954	1952	1954
PMe ₃ Cr(CO) ₅	2063	2063	-	1973	1949	1949	1941	-
PMe ₃ Mo(CO) ₅	2071	2071	-	1981	1952	1952	1945	-
PMe ₃ W(CO) ₅	2071	2072	-	1972	1947	1947	1937	-
AsMe ₃ Cr(CO) ₅	2063	2062	-	1976	1946	1945	1940	-
AsMe ₃ Mo(CO) ₅	2072	2071	-	1983	1948	1947	1948	1948
AsMe ₃ W(CO) ₅	2071	2070	-	1975	1943	1942	1939	1942
PPh ₃ Cr(CO) ₅	2064	2064	1982	1982	1948	1948	1944	-
PPh ₃ Mo(CO) ₅	2073	2074	1989	1989	1951	1951	1951	1951
PPh ₃ W(CO) ₅	2072	2072	1980	1980	1951	1946	1942	-
AsPh ₃ Cr(CO) ₅	2065	2065	1983	1983	1946	1944	1946	1944
AsPh ₃ Mo(CO) ₅	2074	2074	1989	1989	1952	1945	1952	-
AsPh ₃ W(CO) ₅	2073	2073	1981	1981	1944	1943	1944	1943
SbPh ₃ Cr(CO) ₅	2062	2062	1982	1982	1951	1950	1946	-
SbPh ₃ Mo(CO) ₅	2074	2073	1990	1990	1954	1951	1954	1951
SbPh ₃ W(CO) ₅	2073	2071	1981	1981	1947	1947	1947	1947
qucdCr(CO) ₅ ^e	2065	2063	-	1970	1915	1911	1932	1929
qucdMo(CO) ₅ ^c	2072	2071	-	1974	1917	1915	1936	1934
qucdW(CO) ₅ ^c	2070	2069	-	1970	1916	1912	1927	-
NMe ₃ Cr(CO) ₅ ^d	2067	-	-	-	1917	-	1934	-
NMe ₃ Mo(CO) ₅ ^d	2074	-	-	-	1918	-	1936	-
NMe ₃ W(CO) ₅	2072	2070	-	1966	1918	1915	1930	-

^a The infrared spectra of the present study are consistent with the notion that the B₁ band is activated when L is bulky or asymmetric.

^b Tetrahydrofuran solution; a very weak B₁ band is observed.

^c The abbreviation qucd represents quinuclidine.

^d Raman spectra were not obtained due to decomposition of the sample upon prolonged exposure to the laser.

From the carbonyl band positions in Table 1, it is seen that $\nu(\text{CO})$ can vary extensively with change of ligand L. The $\nu(\text{CO})$ absorptions are sensitive to the electronic population of the carbonyl π^* molecular orbitals and this is determined largely by the electronic properties of the ligand L.²⁰ The $\nu(\text{CO})$ bands generally decrease down the table as L changes from strongly π -acid ligands to π -neutral tertiary amine ligands.

The band position of $\nu(\text{CO})A_{1\text{eq}}$ for $\text{LCr}(\text{CO})_5$ is found to be lower than for Mo and W analogues which are virtually the same. The $\nu(\text{CO})E$ for tungsten derivatives is at lower energy than for the analogous Cr and Mo complexes.[‡] These trends indicate a qualitatively similar metal dependence within the triad irrespective of the nature of the unique ligand L.

In examining the bonding interactions between M and L in $\text{LM}(\text{CO})_5$, many workers have used the so-called "characteristic CO stretching frequency", *i.e.* that of $A_{1\text{eq}}$, to probe the σ -donor/ π -acceptor properties of the ligand L.^{10,22-26} However, as shown from the plots of experimental data in Fig. 2, the carbonyl mode most affected by change of L is $\nu(\text{CO})A_{1\text{ax}}$.

According to Cotton and Kraihanzel,⁸ the two dominant contributions to $\nu(\text{CO})$ in $\text{LM}(\text{CO})_5$ complexes are the σ -donor and π -acceptor capacities of L. Using arguments in refs. 8, 27 and 28, the σ component should affect the three metal t_{2g} d_π orbitals equally and thus is isotropic. The π component, in contrast, has directional properties,⁸ more affecting the CO ligand *trans* to L than those *cis* to L. This is because the *trans* CO interacts with two d_π orbitals in common with L, whereas each *cis* CO ligand shares only one metal d_π orbital. The $A_{1\text{ax}}$ carbonyl absorption should therefore reflect the π -accepting ability of L more sensitively than the $A_{1\text{eq}}$ mode.

[‡] The band patterns for $\nu(\text{CO})A_{1\text{eq}}$ and for $\nu(\text{CO})E$ are respectively similar to those of $\nu(\text{CO})A_{1g}$ and $\nu(\text{CO})T_{1u}$ for $\text{M}(\text{CO})_6$, from which they are derived.²¹

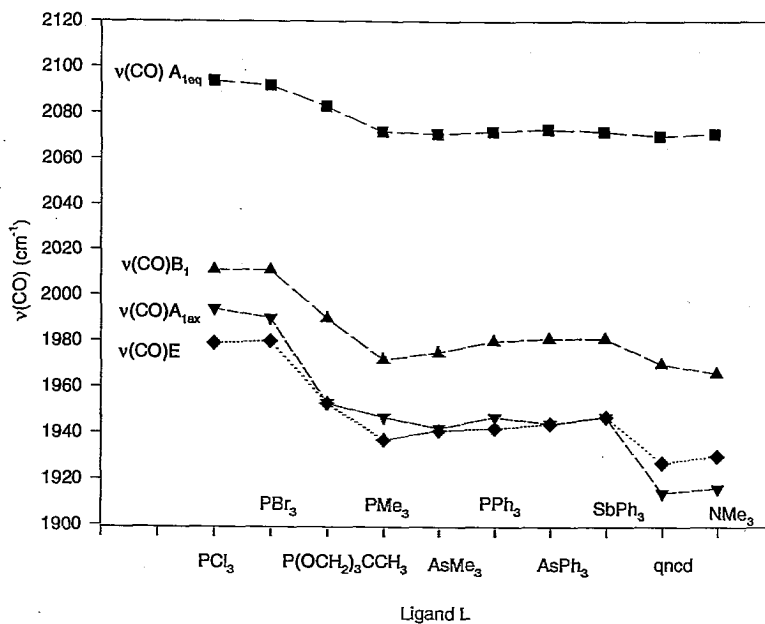


Fig. 2 Variation of $v(CO)$ with change in ligand L in $LW(CO)_5$ complexes.

Comparisons of the A_{1ax} and A_{1eq} band positions provide some insight into the M-L π component, since the σ components should be relatively close for these modes for any given ligand. In Fig. 3, $v(CO)A_{1ax}$ is plotted against $v(CO)A_{1eq}$ using the data for the tungsten complexes in Table 1. Analogous plots for the Cr and Mo complexes (not shown) are very similar. The trends for these groupings indicate the usually accepted M-L π bonding order $PCl_3 \sim PBr_3 > P(OCH_2)_3CCH_3 > EPh_3 \sim EMe_3 > qncd \sim NMe_3$. Alternative interpretations attributing such trends predominantly to σ -donor properties of L have largely been discredited.²⁹⁻³³

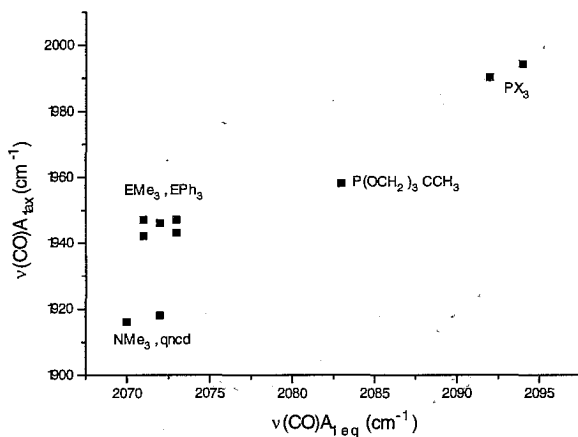


Fig. 3 Plot of $\nu(\text{CO})A_{1\text{eq}}$ vs $\nu(\text{CO})A_{\text{max}}$ for $\text{LW}(\text{CO})_5$.

Infrared and Raman spectra of $\text{LM}(\text{CO})_5$ complexes in the metal-carbon stretching region

For these complexes, $\nu(\text{MC})$ is more difficult to assign than $\nu(\text{CO})$. This is due to much lower infrared intensities for $\nu(\text{MC})$, the presence in this region of other bands including deformation vibrations such as $\delta(\text{MCO})$ as well as intra-ligand vibrations, and also the complication of lower vibrational purity due to mechanical coupling between different vibrational modes of the same symmetry.

The band assignments in Table 2 were made by comparison of the infrared and Raman spectra over the region studied and also with reference to previous literature assignments.^{7,29,34-40} The $\nu(\text{MC})$ mode of E symmetry was obtained in each case from the infrared spectrum; this band has high intensity. The two bands of A_1 symmetry were assigned from polarised Raman spectra. Those of B_1 symmetry were identified as peaks of very low intensity in the infrared and as depolarised Raman bands. A strong metal dependence is evident for the $\nu(\text{MC})$ vibrations.

Table 2 Infrared and Raman Metal-Carbon Band Positions
for $LM(CO)_5$ Complexes in Cyclopentane (cm^{-1}).^a

Complex	$\nu(MC)A_{1eq}$		$\nu(MC)B_1$		$\nu(MC)A_{1ax}$		$\nu(MC)E$	
	IR	R	IR	R	IR	R	IR	R
$PCl_3Cr(CO)_5$	384	385	405	395	432	431	454	-
$PCl_3W(CO)_5$	423	423	-	-	401	400	375	-
$PBr_3Cr(CO)_5$	384	383	-	430	420	419	463	-
$PBr_3W(CO)_5$	444	443	418	-	426	416	373	-
$P(OCH_2)_3CCH_3Cr(CO)_5$	405	395	420	407	454	450	470	-
$P(OCH_2)_3CCH_3Mo(CO)_5$	419	-	-	-	408	408	378	-
$P(OCH_2)_3CCH_3W(CO)_5$	448	-	-	420	425	433	386	-
$PMe_3Cr(CO)_5$	-	397	-	409	-	462	467	-
$PMe_3Mo(CO)_5$	394	402	-	-	411	415	382	-
$PMe_3W(CO)_5$	-	436	414	414	426	425	387	-
$AsMe_3Cr(CO)_5$	-	396	-	407	-	465	467	-
$AsMe_3Mo(CO)_5$	397	404	-	394	424	424	380	-
$AsMe_3W(CO)_5$	444	441	411	412	429	429	386	-
$PPh_3Cr(CO)_5$	388	394	410	405	-	464	465	-
$PPh_3Mo(CO)_5$	401	402	-	-	-	432	378	-
$PPh_3W(CO)_5$	447	444	-	-	-	427	383	-
$AsPh_3Cr(CO)_5$	388	394	-	405	-	466	470	-
$AsPh_3Mo(CO)_5$	396	401	-	395	433	433	378	-
$AsPh_3W(CO)_5$	-	447	-	421	428	427	384	-
$SbPh_3Cr(CO)_5$	386	394	-	406	-	466	453	-
$SbPh_3Mo(CO)_5$	430	429	-	394	398	401	379	-
$SbPh_3W(CO)_5$	447	445	-	421	-	427	386	-
$qncdCr(CO)_5$	388	385	-	394	-	481	442	439
$qncdMo(CO)_5$	-	466	-	-	404	404	366	-
$qncdW(CO)_5$	-	-	407	-	428	-	372	-
$NMe_3W(CO)_5$	-	465	-	-	-	427	-	-

^a Some bands are not observed in the spectra despite being formally allowed by symmetry.

The polarisation properties of the $\nu(\text{MC})$ bands differ from the analogous $\nu(\text{CO})$ bands. Both $\nu(\text{MC})A_1$ bands are completely polarised; $\nu(\text{CO})A_{1\text{eq}}$ is completely polarised but $\nu(\text{CO})A_{1\text{ax}}$ is not. This is probably due to greater vibrational mixing in $\nu(\text{MC})$ than in $\nu(\text{CO})$.

A qualitative "reciprocal relationship" is seen between $\nu(\text{MC})$ and $\nu(\text{CO})$, *i.e.* higher energy CO vibrations correlate with lower energy MC vibrations, as expected on the basis of the Dewar-Chatt π -bonding model.²⁰ The correlation between analogous MC and CO vibration modes is best for $A_{1\text{ax}}$ in accord with the results of Young *et al.*³⁸; those for the E and $A_{1\text{eq}}$ modes are less well defined.

Raman spectra of the metal-ligand stretching region

The $\nu(\text{ME})$ band positions and relative Raman intensities, where E = N, P, As or Sb, are listed in Table 3. The bands $\nu(\text{ME})$ are observed in the 130 - 220 cm^{-1} region but in the infrared spectra of these complexes the absorptions are very weak and difficult to separate from the background noise. For this reason the corresponding Raman spectra have been used to assign these bands. The band positions are, however, an inadequate measure of the M-L bond strength since the masses of the ligands (and thus the reduced masses) vary greatly. An additional complication involves gauging the effective mass of the ligand, particularly for flexible species like PPh_3 .

In the absence of an accurate normal coordinate analysis on these complexes comparisons can only be qualitative. The only such study on complexes $\text{PY}_3\text{M}(\text{CO})_5$ is that by Poilblanc and his coworkers⁴¹ on $\text{PH}_3\text{M}(\text{CO})_5$. Similar studies on $\text{Mn}(\text{CO})_5\text{X}$ (X = halogen or Me)⁴² and on $\text{PY}_3\text{Ni}(\text{CO})_3$ (Y = F, Me or OMe)⁴³ indicate that the M-P force constant lies in the region of 1.2 - 1.35 ($\times 10^2 \text{ Nm}^{-1}$) for PMe_3 and is even greater for $\text{P}(\text{OMe})_3$ and PF_3 .

Table 3 Metal-Ligand Band Positions (cm^{-1}) and Relative Raman Intensities for $\text{EY}_3\text{M}(\text{CO})_5$ Complexes.^a

Complex	$\nu(\text{ME})$	Relative intensity
$\text{PBr}_3\text{Cr}(\text{CO})_5$	211	1.872 ^b
$\text{PBr}_3\text{W}(\text{CO})_5$	198	1.060 ^b
$\text{P}(\text{OCH}_2)_3\text{CCH}_3\text{Cr}(\text{CO})_5$	215	0.327 ^c
$\text{P}(\text{OCH}_2)_3\text{CCH}_3\text{Mo}(\text{CO})_5$	190	0.135 ^c
$\text{P}(\text{OCH}_2)_3\text{CCH}_3\text{W}(\text{CO})_5$	177	0.139 ^c
$\text{PMe}_3\text{Cr}(\text{CO})_5$	222	0.317 ^d
$\text{PMe}_3\text{Mo}(\text{CO})_5$	204	0.111
$\text{PMe}_3\text{W}(\text{CO})_5$	198	0.116
$\text{AsMe}_3\text{Cr}(\text{CO})_5$	194	0.479
$\text{AsMe}_3\text{Mo}(\text{CO})_5$	175	0.228
$\text{AsMe}_3\text{W}(\text{CO})_5$	167	0.229
$\text{PPh}_3\text{Cr}(\text{CO})_5$	185	0.345 ^d
$\text{PPh}_3\text{Mo}(\text{CO})_5$	169	0.171
$\text{PPh}_3\text{W}(\text{CO})_5$	160	0.179
$\text{AsPh}_3\text{Cr}(\text{CO})_5$	174	0.479
$\text{AsPh}_3\text{Mo}(\text{CO})_5$	155	0.224
$\text{AsPh}_3\text{W}(\text{CO})_5$	145	0.239
$\text{SbPh}_3\text{Cr}(\text{CO})_5$	172	0.844
$\text{SbPh}_3\text{Mo}(\text{CO})_5$	150	0.255
$\text{SbPh}_3\text{W}(\text{CO})_5$	137	0.305
$\text{qncdCr}(\text{CO})_5$	176	e
$\text{qncdMo}(\text{CO})_5$	169	e
$\text{qncdW}(\text{CO})_5$	165	e
$\text{NMe}_3\text{Cr}(\text{CO})_5$	211	e
$\text{NMe}_3\text{W}(\text{CO})_5$	205	e

^a Spectra were recorded using the Ar^+ 514.5 nm exciting line, for cyclopentane solutions.

- ^b Spectra were recorded using the Kr⁺ 647.1 nm exciting line as these compounds are slightly more coloured than the others examined. This excitation line is sufficiently distant from any region of electronic absorption to eliminate the possibility of pre-resonance enhancement. Intensities can be corrected to those for the 514.5 nm line by multiplying them by 2.5 (see footnote *d*).
- ^c Spectra were recorded in THF using Kr⁺ 647.1 nm and intensities can be corrected to those for 514.5 nm as in (*b*). Comparison of intensities is not feasible as spectra of $\text{PMe}_3\text{Cr}(\text{CO})_5$ and $\text{PPh}_3\text{Cr}(\text{CO})_5$ in THF show substantial band width increases indicating interaction with the solvent.
- ^f Spectra were recorded as well at 647.1 nm to enable comparison against $\text{PBr}_3\text{M}(\text{CO})_5$ and to ensure that there were no pre-resonance effects operating in the spectra of the complexes recorded at 514.5 nm. Intensities for 647.1 nm radiation are as follows: $\text{PMe}_3\text{Cr}(\text{CO})_5$ 0.124, $\text{PPh}_3\text{Cr}(\text{CO})_5$ 0.128. To a good approximation, the Raman band intensity is proportional to the fourth power of the frequency of the exciting line. It is easily shown that a band recorded using 514.5 nm radiation should be 2.5 times as intense as the same band from 647.1 nm excitation radiation.⁴⁴ The band intensities now reported are entirely consistent with this.
- ^e The $\nu(\text{MN})$ band intensities are considerably weaker than $\nu(\text{MP})$ and band fits are unreliable.

Some qualitative trends are apparent in the data of Table 3. The Cr-P vibration in $\text{PMe}_3\text{Cr}(\text{CO})_5$ is found at higher energy than Cr-N observed for $\text{NMe}_3\text{Cr}(\text{CO})_5$. On the basis of the reduced masses, $\nu(\text{MP})$ for $\text{PMe}_3\text{Cr}(\text{CO})_5$ would be expected to have a lower energy than $\nu(\text{MN})$ from $\text{NMe}_3\text{Cr}(\text{CO})_5$; thus the metal-phosphorus bond is stronger than the analogous metal-nitrogen bond.

Within the series of phosphine complexes some direct comparisons can be made. The masses of the triphenylphosphine and phosphorus tribromide ligands are very close, and so the band position of the M-P vibration (to a first approximation) should reflect the strength of that particular bond. In both the Cr and W complexes the PBr_3 derivative is found to have $\nu(\text{MP})$ at higher energy than for the analogous PPh_3 derivative. Thus it is concluded that the metal-phosphorus bond is stronger for the phosphorus tribromide complexes than in the triphenylphosphine derivatives. The implication here is that there is a strong π component in the M-P bond especially in the case of the PBr_3 complexes as triphenylphosphine is believed to be a better σ -donor ligand.²⁰ This correlates well with conclusions obtained from directional polarisability studies and from X-ray crystallographic analyses recently reported in refs. 2 and 6.

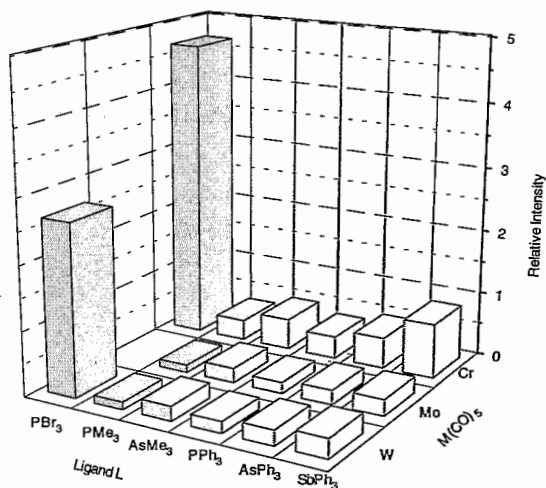


Fig. 4 Raman M-E band intensities for $\text{EY}_3\text{M}(\text{CO})_5$ complexes.*

Listed also in Table 3 are the relative molar Raman intensities of $\nu(\text{ME})$ and these are compared in Fig. 4. To a first approximation, the intensity of a Raman band can be taken as a measure of the polarisability change of the bond undergoing a vibration.[#] It has been shown that trends in Raman intensities can be interpreted to give some insight into the covalent nature of a bond.⁴⁵ Since π electrons contribute far more to the derived bond polarisability than do σ electrons^{45,46}, high Raman band intensities have been taken to indicate substantial π -bond character.

It is seen that the M-E band intensity increases as E descends the group ($\text{P} < \text{As} < \text{Sb}$) *i.e.* with increasing size and polarisability of the donor atom E. In all cases the Cr complexes have higher M-E band intensities than do the molybdenum and tungsten analogues.

* The M-P band intensities for $\text{PBr}_3\text{M}(\text{CO})_5$ are corrected for the frequency of the excitation line and are 2.5 times the values shown in Table 3.

[#] Strictly, the Raman intensities are a measure of the change in polarisability α with change in vibrational state along a normal coordinate Q , *i.e.* $(\partial\alpha/\partial Q)_0$ measured at the equilibrium position.

Of particular importance is the observation that the M-P band intensity for $\text{PBr}_3\text{M}(\text{CO})_5$ is very much greater than for the trialkyl- and triaryl-phosphine analogues. This is strong evidence for greatly enhanced metal-phosphorus π bonding in the phosphorus tribromide complexes resulting from the highly electronegative bromo-substituents in the phosphine ligand. It accords with the vibration energies earlier discussed and with conclusions in refs. 2 and 6. The $\text{P}(\text{OCH}_2)_3\text{CCH}_3\text{M}(\text{CO})_5$ complexes deserve comment in that the oxygens of the ligand are constrained with P-O-C bond angles of *ca.* 115° ,³ the appreciable sp^2 character favours drift of electron density from the largely unhybridised filled *p* orbital on each oxygen into available *d* orbitals of phosphorus.⁴⁷ This results in a less than expected π interaction between M and the phosphorus ligand.

For all cases examined, the corresponding pairs of EMe_3 - and $\text{EPh}_3\text{M}(\text{CO})_5$ complexes have similar M-E intensities, consistent with earlier suggestions that the EMe_3 and EPh_3 ligands in these complexes exhibit very similar bonding properties.^{4,20,48} The intensities of the M-N bands for $\text{qncdM}(\text{CO})_5$ and $\text{NMe}_3\text{M}(\text{CO})_5$ are much lower than observed for the same metal in the phosphine complexes. This may be partly due to the smaller size and harder, less polarisable N donor atom, but the lack of π character for M-N is undoubtedly an important factor.

The low-wavenumber region of the vibrational spectra of the $\text{PCl}_3\text{M}(\text{CO})_5$ complexes presents special difficulties. The infrared and Raman spectra of these complexes differ in many respects from those of the other $\text{LM}(\text{CO})_5$ compounds. The infrared spectra exhibit a strong absorption in the 300 - 310 cm^{-1} region. A strong polarised band is found in the same position in the Raman spectra. This band has been "tentatively assigned" as $\nu(\text{CrP})$ in $\text{PCl}_3\text{Cr}(\text{CO})_5$ by Boxhoorn *et al.*³⁵ and as $\nu(\text{CrC})\text{A}_{1\text{eq}}$ by Guns, Claeys and van der Kelen.³⁷ Clearly, doubt exists about the identity of this band. A knowledge of the infrared and Raman spectra of "free" PCl_3 is valuable in making band assignments for the metal carbonyl derivatives. The fundamental vibrations of free PCl_3 are: $\nu_s(\text{PCl})\text{A}_1$ 515 cm^{-1} , $\delta_s(\text{PCl}_3)\text{A}_1$ 258 cm^{-1} , $\nu_{\text{as}}(\text{PCl})\text{E}$ 504 cm^{-1} and $\delta_{\text{as}}(\text{PCl}_3)\text{E}$ 186 cm^{-1} , as reported by Clark and Rippon.⁴⁹ The spectra of the $\text{PCl}_3\text{M}(\text{CO})_5$ complexes exhibit bands at 512 - 514 cm^{-1} , but other bands which could correspond to those of free PCl_3 are not seen in either the infrared or Raman spectra. An insight into the absence of these bands comes from a vibrational analysis by Edwards and Woodward⁵⁰ on $(\text{PCl}_3)_4\text{Ni}$. A strong polarised band in the Raman spectrum of $(\text{PCl}_3)_4\text{Ni}$ at 306 - 310 cm^{-1} , not seen in the infrared spectrum, was

assigned as $\delta_s(\text{PCl}_3)$ and a band at 208 cm^{-1} was assigned as $\nu(\text{NiP})$. Force constant calculations were made which showed that $\nu_s(\text{PCl})$ "involves a large amount of Ni-P stretching and P-Cl stretching".

As earlier noted, $\text{PBr}_3\text{M}(\text{CO})_5$ compounds exhibit an exceptionally strong polarised Raman band at 211 cm^{-1} and 198 cm^{-1} for $\text{M} = \text{Cr}$ and W , respectively. This is now assigned as $\nu(\text{MP})$. It can be shown using reduced masses that $\nu(\text{MP})$ for $\text{PCl}_3\text{M}(\text{CO})_5$ complexes may be almost degenerate with $\delta_s(\text{PCl})^*$ and so extensive mixing of the two vibrations is expected. It is proposed that bands found at 307 cm^{-1} and 196 cm^{-1} for $\text{PCl}_3\text{Cr}(\text{CO})_5$ and at 301 cm^{-1} and 167 cm^{-1} for $\text{PCl}_3\text{W}(\text{CO})_5$ are linear combinations of the $\nu(\text{MP})$ and $\delta_s(\text{PCl}_3)$ vibrations. An alternative explanation that the lower energy bands for each metal complex have solely metal-phosphorus stretch character is rejected on the grounds that the force constant between M and P would be far lower for PCl_3 than for PBr_3 . This is not indicated by other results in this work which suggest almost identical behaviour for the coordinated PCl_3 and PBr_3 ligands. The M-P band positions in complexes of PBr_3 would be expected to occur at lower energies due to the greater mass of this ligand.

The effect on $\nu(\text{EY})$ of EY_3 complexation

The classical model of π -backbonding involving the electron drift from metal M to empty d orbitals of the ligand σ -donor atom E ($\text{E} = \text{P}, \text{As}$ or Sb) is currently under challenge. Recently published work has suggested that the coordinated EY_3 ligands accept electrons from M into antibonding $\text{E-Y } \sigma^*$ receptor orbitals or these in combination with d orbitals of E .⁵¹⁻⁵⁷ This is now explored by studying the effect of EY_3 coordination on the E-Y band frequency.

The EY_3 grouping as such has three-fold symmetry (ignoring for the moment the E substituent groups). The E-Y stretching vibrations have A_1 and E modes and the

* Assuming that the metal-phosphorus force constant is the same for the $\text{PCl}_3\text{M}(\text{CO})_5$ and $\text{PBr}_3\text{M}(\text{CO})_5$ complexes and that the entire $\text{M}(\text{CO})_5$ moiety is involved in the vibration, substituting the appropriate mass of PCl_3 in place of PBr_3 gives an estimated $\nu(\text{MP})$ of $\sim 250\text{ cm}^{-1}$. This is reasonable since the M-PCl_3 and M-PBr_3 bond lengths are almost identical and the carbonyl band positions are very similar for the two $\text{PX}_3\text{M}(\text{CO})_5$ complexes.

Y-E-Y deformation vibrations also have A_1 and E species. By treating the $M(CO)_5$ as a point mass, and assuming negligible interaction between M-C vibrations and those of EY_3 , coordination of EY_3 to $M(CO)_5$ does not alter the symmetry. The M-E stretch in $EY_3M(CO)_5$ has A_1 symmetry, and so vibrational mixing between E-Y and M-E will be restricted to the modes of A_1 symmetry. The frequencies of the E-Y stretches are listed for the free EY_3 ligands, their oxides, borane adducts and the $EY_3M(CO)_5$ complexes in Table 4.

Table 4 Band Positions (cm^{-1}) of $\nu(EY)$ and $\delta(YEY)$ for the EY_3 Moiety in the Free and Complexed State.

Compound	$\nu_s(EY) A_1$	$\nu_{as}(EY) E$	$\delta_s(YEY) A_1$	$\delta_{as}(YEY) E$
$PMe_3^{a,b}$	653	708	305	263
$OPMe_3^a$	665	734	311	256
$PMe_3BCl_3^c$	664	738	300	269
$PMe_3Cr(CO)_5$	675	-	343	-
$PMe_3Mo(CO)_5$	670	-	337	-
$PMe_3W(CO)_5$	672	-	340	-
$AsMe_3^{b,d}$	567	582	236	221
$AsMe_3BCl_3^e$	595	640	210	229
$AsMe_3BBr_3^e$	587	636	209	227
$AsMe_3BI_3^e$	580	632	209	220
$AsMe_3Cr(CO)_5$	586	607	253	220
$AsMe_3Mo(CO)_5$	586	605	249	219
$AsMe_3W(CO)_5$	587	606	249	218
PBr_3^f	390	384	159	113
$PBr_3Cr(CO)_5$	383	383	148	-
$PBr_3W(CO)_5$	386	386	140	120

^a From ref. 58.

^b From ref. 59.

^c From ref. 60.

^d From ref. 61.

^e From ref. 62.

^f From ref. 49.

The band position of $\nu(\text{EY})$ should, in principle, be sensitive to the population of the $\text{E-Y } \sigma^*$ orbital; weakening of the bond should result in a lowering of the stretching frequency. The data show a small increase in the energy of the P-Me and As-Me stretches upon complexation to BX_3 or $\text{M}(\text{CO})_5$; very little change occurs with P-Br .

Normal coordinate analyses on OPMe_3 and the borane adducts of AsMe_3 indicate that the E-C force constants are greater in the coordinated ligand than in free EMe_3 .⁵⁸⁻⁶³ Comparison of the band positions of the borane adducts and the corresponding $\text{LM}(\text{CO})_5$ complexes shows that for $\text{L} = \text{PMe}_3$ the energies of both the symmetric P-C stretching vibrations and C-P-C deformations are greater in the latter compounds; that for As-C remains virtually the same and the C-As-C deformation is at higher energy in the metal carbonyl complexes. The results are tentative in the absence of accurate force constant data from normal coordinate analysis. Overall, they suggest that there is no weakening of the $\text{E-Y } \sigma$ bond with coordination of EY_3 . This is in concordance with recent bond distance studies⁶ of $\text{PY}_3\text{M}(\text{CO})_5$ complexes which indicate little involvement of $\text{P-Y } \sigma^*$ antibonding orbitals in the π -backdonation mechanism.

CONCLUSIONS

Trends in the band vibrational frequencies and intensities of $\text{LM}(\text{CO})_5$ complexes have been analysed to ascertain, more definitively than before, the relative π -backbonding abilities of ligands L . The high order of polarisability found for bonds between M and PBr_3 provides convincing evidence for substantial π character, consistent with the postulate of π -acceptor ability for this ligand. The results suggest little involvement of $\text{E-Y } \sigma^*$ antibonding orbitals in the receptor mechanism for π -backbonding to coordinated EY_3 .

ACKNOWLEDGEMENTS

Assistance from Dr. Bradley Collins is gratefully acknowledged.

ΠΕΡΙΛΗΨΗ

LM(CO)₅ ΣΥΜΠΛΟΚΑ ΜΕ π-ΔΕΣΜΟ ΜΕΤΑΛΛΟΥ-ΥΠΟΚΑΤΑΣΤΑΤΗ: ΜΕΛΕΤΗ ΔΟΝΗΤΙΚΗΣ ΦΑΣΜΑΤΟΣΚΟΠΙΑΣ

Στο παρόν άρθρο παρουσιάζεται συστηματική μελέτη των θέσεων των ταινιών απορροφήσεως υπέρυθρου και Raman και των σχετικών εντάσεων των ταινιών απορροφήσεως ορισμένων χαρακτηριστικών δονήσεων για μια σειρά συμπλόκων του τύπου LM(CO)₅ (L είναι αμίνη, φωσφίνη ή σχετικός υποκαταστάτης, M είναι μέταλλο της τριάδας του χρωμίου). Τα δεδομένα αναλύονται με σκοπό να επιβεβαιώσουν ακριβέστερα από ότι προηγούμενες μελέτες, τις σχετικές δυνατότητες του υποκαταστάτη για το σχηματισμό π-δεσμών. Από τις εντάσεις των ταινιών Raman ευρέθη μία υψηλής τάξεως πολωσιμότητα για τους δεσμούς μεταξύ M και PBr₃, παρέχοντας έτσι μία ισχυρή ένδειξη για την ύπαρξη σημαντικών π-χαρακτήρα δεσμών. Τα αποτελέσματα επίσης υποδεικνύουν μικρή συμμετοχή των E-Y σ* αντιδεσμικών τροχιακών στο μηχανισμό για την π-οπισθοσύνδεση του υποκαταστάτη προς το συμπλεγμένο EY₃.

REFERENCES

1. M.J. Aroney, R.M. Clarkson, T.W. Hambley and R.K. Pierens, *J. Organomet. Chem.*, 426 (1992) 331.
2. M.S. Davies, R.K. Pierens and M.J. Aroney, *J. Organomet. Chem.*, 458 (1993) 141.
3. M.J. Aroney, M.S. Davies, T.W. Hambley and R.K. Pierens, *J. Chem. Soc. Dalton Trans.*, (1994) 91.
4. M.S. Davies, G.W. Allen, M.J. Aroney, T.W. Hambley and R.K. Pierens, *J. Mol. Struct.*, 326 (1994) 81.
5. M.J. Aroney, I.E. Buys, M.S. Davies and T.W. Hambley, *J. Chem. Soc. Dalton Trans.*, (1994) 2827.
6. M.S. Davies, M.J. Aroney, I.E. Buys, T.W. Hambley and J.L. Calvert, *Inorg. Chem.*, 34 (1995) 330.

7. R. Poiblanç and M. Bigorgne, *Bull. Soc. Chim. Fr.*, (1962) 1301.
8. F. A. Cotton and C. S. Kraihanzel, *J. Am. Chem. Soc.*, **84** (1962) 4432.
9. D. J. Darensbourg and T. L. Brown, *Inorg. Chem.*, **7** (1968) 959.
10. F. T. Delbecke and G. P. van der Kelen, *J. Organomet. Chem.*, **64** (1974) 239.
11. T. L. Brown and D. J. Darensbourg, *Inorg. Chem.*, **6** (1967) 971.
12. S. F. A. Kettle and I. Paul, *Inorg. Chim. Acta*, **2** (1968) 15.
13. J. R. Miller, *Inorg. Chim. Acta*, **2** (1968) 421.
14. D. M. Adams, *Metal-Ligand and Related Vibrations*, Arnold, London, 1967, pp. 97-103, 107-109.
15. M.S. Davies, PhD Thesis, University of Sydney, 1994.
16. L.E. Orgel, *Inorg. Chem.*, **1** (1962) 25.
17. S. F. A. Kettle, I. Paul and P. J. Stamper, *J. Chem. Soc. Dalton Trans.*, (1972) 2413.
18. A. M. English, K. R. Plowman and I. S. Butler, *Inorg. Chem.*, **20** (1981) 2553.
19. M. Bigorgne, *Spectrochim. Acta*, **32A** (1976) 1365.
20. J.E. Huheey, *Inorganic Chemistry*, 3rd ed., Harper and Row, Cambridge, 1983, pp. 433-438.
21. L.H. Jones, R.S. McDowell and M. Goldblatt, *Inorg. Chem.*, **8** (1969) 2349.
22. E. Vincent, L. Verdonck, D. F. van de Vondel and G. P. van der Kelen, *J. Mol. Struct.*, **112** (1984) 119.
23. E. Vincent, L. Verdonck and G. P. van der Kelen, *J. Mol. Struct.*, **69** (1980) 33.
24. L. Verdonck, E. Vincent and G. P. van der Kelen, *J. Mol. Struct.*, **117** (1984), 257.
25. G. R. Dobson, *Acc. Chem. Res.*, **9** (1976) 300.
26. R. J. Angelici and M. D. Malone, *Inorg. Chem.*, **6** (1967) 1731.
27. W. A. G. Graham, *Inorg. Chem.*, **7** (1968) 315.
28. F. A. Cotton and R. M. Wing, *J. Organomet. Chem.*, **9** (1967) 511.
29. R. A. Brown and G. R. Dobson, *Inorg. Chim. Acta*, **6** (1972) 65.
30. M.M. Rahman, H.Y. Liu, K. Eriks, A. Prock and W.P. Giering, *Organometallics*, **8** (1989) 1.
31. L.M. Haines and M.H.B. Stiddard, *Adv. Inorg. Chem. Radiochem.*, **12** (1969) 53.
32. R.P. Stewart and P.M. Treichel, *Inorg. Chem.*, **7** (1968) 1942.
33. R.J. Dennenberg and D.J. Darensbourg, *Inorg. Chem.*, **11** (1972) 72.
34. S. Singh, P. P. Singh and R. Rivest, *Inorg. Chem.*, **7** (1968) 1236.
35. G. Boxhoorn, D. J. Stufkens and A. Oskam, *Inorg. Chim. Acta*, **33** (1979) 215.
36. A. C. Vandenbroucke, D. G. Hendricker, R. E. McCarley and J. G. Verkade, *Inorg. Chem.*, **7** (1968) 1825.

37. M. F. Guns, E. G. Claeys and G. P. van der Kelen, *J. Mol. Struct.*, 65 (1980) 3.
38. F. R. Young, R. A. Levenson, M. N. Memering and G. R. Dobson, *Inorg. Chim. Acta*, 8 (1974) 61.
39. G. Boxhoorn and A. Oskam, *Inorg. Chim. Acta*, 29 (1978) 243.
40. A. A. Chalmers, J. Lewis and R. Whyman, *J. Chem. Soc. A*, (1967) 1817.
41. C. Jeanne, R. Pince and R. Poilblanc, *Spectrochim. Acta*, 31A (1975) 819.
42. H. D. Kaesz, R. Bau, D. Hendrickson and J. M. Smith, *J. Am. Chem. Soc.*, 89 (1967) 2844.
43. M. Bigorgne, A. Loutellier and M. Pankowski, *J. Organomet. Chem.*, 23 (1970) 201.
44. D.A. Long, *Raman Spectroscopy*, McGraw-Hill, New York, 1977, p. 102.
45. R. S. Armstrong, M. J. Aroney, C. M. Barnes and K. W. Nugent, *J. Mol. Struct.*, 323 (1994) 15.
46. G. W. Chantry and R. A. Plane, *J. Chem. Phys.*, 33 (1960) 634.
47. J.G. Verkade, *Coord. Chem. Rev.*, 9 (1972/73) 1.
48. G.M. Bancroft, L. Dignard-Bailey and R.J. Puddephatt, *Inorg. Chem.*, 25 (1986) 3675.
49. R.J.H. Clark and D.M. Rippon, *J. Mol. Spectrosc.*, 52 (1974) 58.
50. H.M.G. Edwards and L.A. Woodward, *Spectrochim. Acta*, 26A (1970) 1077.
51. R.H. Crabtree, *The Organometallic Chemistry of the Transition Metals*, 2nd ed., Wiley-Interscience, New York, 1994, pp. 83-85.
52. G. Pacchioni and P.S. Bagus, *Inorg. Chem.*, 31 (1992) 4391 (and references cited therein).
53. S.X. Xiao, W.C. Trogler, D.E. Ellis and Z. Berkovitch-Yellin, *J. Am. Chem. Soc.*, 105 (1983) 7033.
54. A.G. Orpen and N.G. Connelly, *Organometallics*, 9 (1990) 1206.
55. A.G. Orpen and N.G. Connelly, *J. Chem. Soc., Chem. Commun.*, (1985) 1310.
56. D.S. Marynick, *J. Am. Chem. Soc.*, 106 (1984) 4064.
57. S.T. Krueger, R. Poli, A.L. Rheingold and D.L. Staley, *Inorg. Chem.*, 28 (1989) 4599.
58. W. Schneider, W. Thiel and A. Komornicki, *J. Phys. Chem.*, 92 (1988) 5611.
59. G. Bouquet and M. Bigorgne, *Spectrochim. Acta*, 23A (1967) 1231.
60. J. E. Drake, J. L. Hencher and B. Rapp, *Inorg. Chem.*, 16 (1977) 2289.
61. E. G. Claeys and G. P. van der Kelen, *Spectrochim. Acta*, 22 (1966) 2095.
62. J. E. Drake, L. N. Khasrou and A. Majid, *Can. J. Chem.*, 59 (1981) 2417.
63. P. J. D. Park and P. J. Hendra, *Spectrochim. Acta*, 24A (1968) 2081.

CONTENTS

CLIMATE FORCING BY TROPOSPHERIC SULFATE AEROSOLS DERIVED FROM
NATURAL AND ANTHROPOGENIC SOURCES

by N. Mihalopoulos and B.C. Nguyen.....173

MIKTOARM STAR POLYMERS

by N. Hadjichristidis, H. Iatrou, Y. Tselikas,

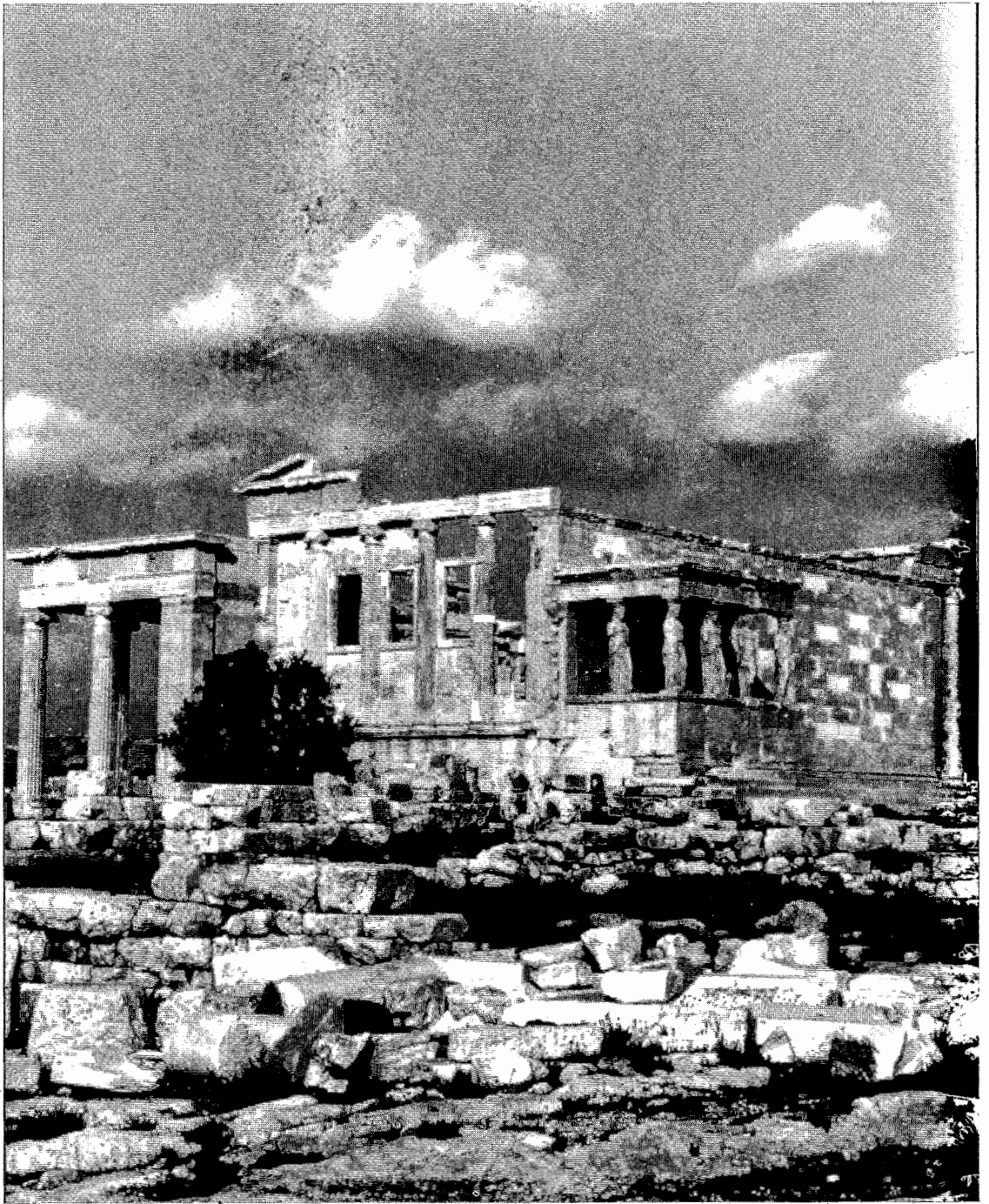
V. Efstratiadis.....189

AN ESR STUDY OF RADICALS AND RADICAL-CATIONS GENERATED FROM
THE REACTION OF SOME METHOXYPHENYL-SUBSTITUTED ALCOHOLS,
ALDEHYDES AND CARBOXYLIC ACIDS WITH HO·, SO⁺, ^tBuO· AND BY
DIRECT PHOTOLYSIS

by A. Valavanidis, B.C. Gilbert and A.C. Whitwood.....217

METAL-LIGAND π BONDING LM(CO)₂ COMPLEXES - A VIBRATIONAL
SPECTROSCOPY STUDY

by M.S. Davies, R.S. Armstrong, M.J. Aroney.....233



ΟΛΥΜΠΙΑΚΗ
ΑΕΡΟΠΟΡΙΑ



ΑΡΧΑΙΑ ΚΟΡΙΝΘΟΣ

ΕΛΛΗΝΙΚΟΣ ΟΡΓΑΝΙΣΜΟΣ ΤΟΥΡΙΣΜΟΥ